Biomaterials Journal
http://www.biomatj.com
Online ISSN: 2812-5045

Type of the Paper (Review Article)

Creep and Sagging of Dental Alloys: A Review

Sherine Sherif Stino [1,*]

[1] Assistant lecturer, Biomaterial Department,Faculty of Dentistry, Cairo University
* Corresponding author e-mail: sherine.stino@dentistry.cu.edu.eg

Citation: ***Sherine Sherif Stino . Creep and Sagging of Dental Alloys: A Review*** *. Biomat. J., 2 (1),1 – 12 (2023).*

https://doi.org/10.5281/znodo.5829408

Received: 25 December 2022
Accepted: 15 January 2023
Published: 31 January 2023

Abstract: Creep is defined as the permanent deformation of a material when subjected to stresses below the yield strength as a function of time and temperature. Creep is normally an undesirable phenomenon and is often a limiting factor in the lifetime of a material. Sag is the permanent deformation potential of long-span metal bridge structures at porcelain-firing temperatures under the influence of the mass of the prosthesis.

Keywords: : *Creep, sag, permanent deformation,*

Creep is defined as the permanent deformation of a material when subjected to stresses below the yield strength as a function of time and temperature. Creep is normally an undesirable phenomenon and is often a limiting factor in the lifetime of a material (1).

The temperature range in which creep deformation may occur differs in various materials. Creep deformation generally occurs when a material is stressed at a temperature near its melting point. If a metal is held at a temperature near its melting point, over a period of time at stresses well below the material's yield strength, permanent deformation can take place and the resulting strain will increase over time. The effects of creep deformation generally become noticeable at approximately 35% of the melting point for metals (2).

I. Creep test:

Creep properties of materials are determined by subjecting a heated specimen to a constant stress for long periods of time during which strain or deformation is monitored, measured, and plotted as a function of elapsed time until the sample breaks. Most of the creep tests are conducted at high temperatures, necessitating an inert gas furnace surrounding the specimen, it is usually done in a temperature-controlled room, to maintain the temperature constant and to ensure constant loading. Creep test measures the progressive rate of deformation of material at high temperature. For metals, most creep tests are conducted in uniaxial tension (3).

When the change of length of specimen (strain) is plotted versus time increments, a creep curve, is obtained, figure1. The relative increase in the elongation is referred to as the (creep) strain. The rate of deformation is called the creep rate ($d\epsilon/dt$), it is the slope of the line in a Creep strain vs. time curve. The resulting creep curve consists of three distinct stages, each of which has its own distinctive strain–time feature. A curve of creep rate versus total

strain shows the large change in creep rate during the creep test. Since the stress and temperature are constant, this variation in creep rate is the result of changes in the internal structure of the material with creep strain and time, figure 2 (2).

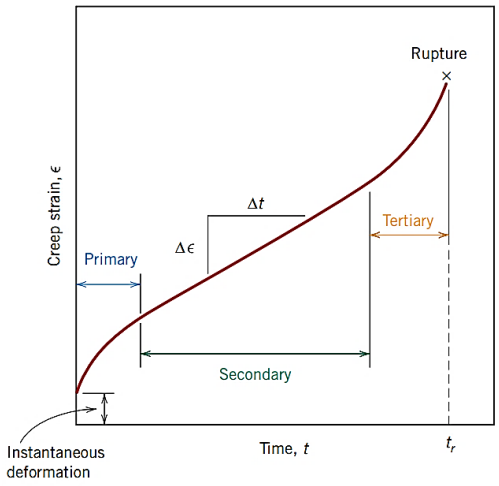

Fig.1: Typical creep curve of strain versus time at constant load and constant elevated temperature.

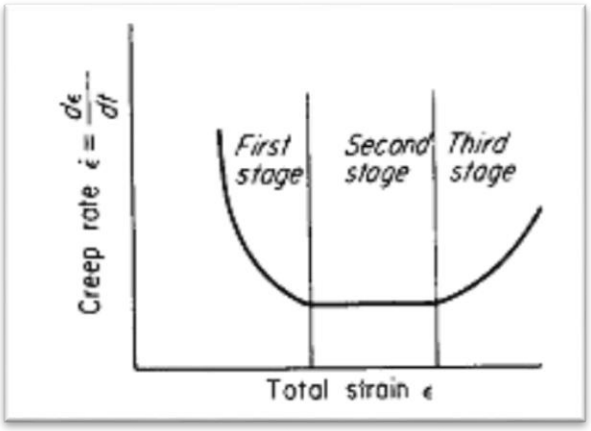

Fig.2: curve of creep rate versus total strain at constant load and constant elevated temperature.

A creep test typically shows these stages:
(i) An initial instantaneous extension or deformation.
(ii) A stage of creep at a decreasing rate.
(iii) A stage of creep at an approximately constant rate.
(iv) A stage of creep at an increasing rate ending in fracture.

Upon load application, at time t = 0, there is first an initial instantaneous deformation, rapid elongation of the specimen, that is totally elastic deformation occurring from atomic bond stretching (2).

(i) Primary or transient creep. During this stage, the strains are relatively small, deformation occurs more rapidly at first and then slows with time. It is characterized by a rapid decrease of creep rate occurring over a relatively short period time until it reaches a constant value, which corresponds to the secondary stage. In metals, this suggests that the material is experiencing strain hardening, where the metal strain-hardens to support the applied load. With further strain hardening, the deformation becomes more difficult as the material is strained and the creep rate decreases with time, the metal is experiencing an increase in creep resistance with strain (2,4).

(ii) Secondary or steady-state creep, (sometimes called linear stage). The strain increases steadily with time, it occurs relatively slow when compared to first and third stages. The creep rate is constant, it has a uniform rate. A linear relationship exists between the strain and the time. It's often the stage of creep that is of the longest duration, where most creep deformation occurs. During this stage, the constancy of creep rate is explained based on a balance between the competing processes of two opposing factors: the strain hardening that tends to reduce the creep rate and the diffusion controlled thermal recovery process (due to the higher temperature) that tends to increase it. Recovery process is slow at low temperature but is rapid at elevated temperature because high thermal energy (high temperature) enhances the atomic diffusion-controlled mechanisms as well involving highly mobile dislocations counteract the strain hardening so that the metal continues to elongate (creep) at a steady constant-state rate. Higher the rate of

recovery the more is the creep deformation, and it becomes significant only at elevated temperatures. No microstructural damage nor fracture will occur at this stage (2,5).

(iii) In the final tertiary stage, it is usually observed at high stresses or/and at high temperatures. A continually increasing creep rate (rapid increase in strain with time) usually spells the beginning of the end of the specimen's test life. As this stage takes place, more and deterioration of the microstructure continues to happen until the material undergo fractures and fails completely. This failure results from microstructural changes or damages such as: grain boundary separation, the formation of internal cracks, voids growth, and, for tensile loads, necking may occur within the deformed region, figure 3. These all lead to a decrease in the effective cross-sectional area (2,6).

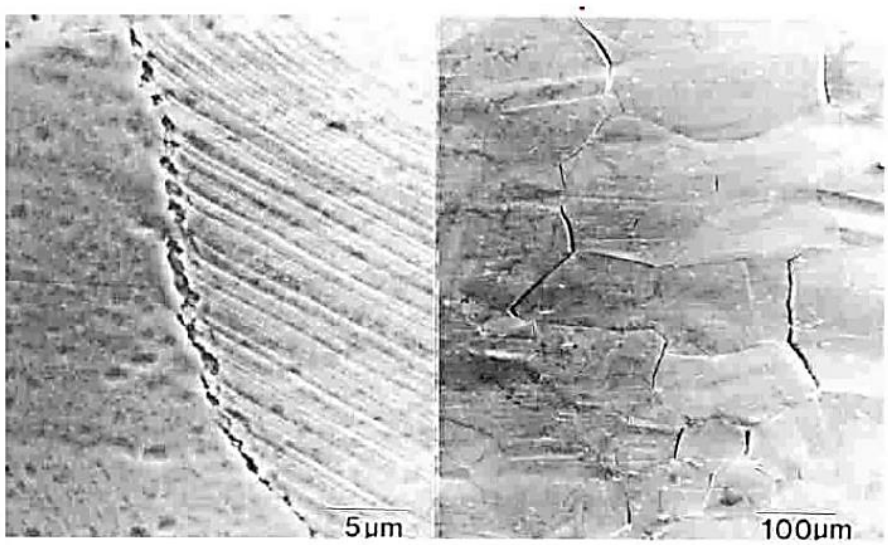

Fig.3: SEM showing voids and cracks on the grain boundary during tertiary creep stage.

II. Effect of temperature and stress on creep of metals:

Both the temperature and the level of the applied stress influence the creep characteristics. It is convenient to refer to the temperature as a function of the melting point temperature Tm on the absolute scale of temperature. Deformation generally occurs when a material is stressed at a temperature near its melting point

The effects of creep deformation of metals and alloys becomes important and generally noticeable when exposed to high temperature, at approximately 35% of the melting point (≈ 0.4 Tm), (Tm is the absolute melting temperature). When the temperature of a metal exceeds 0.4 (T > 0.4Tm), since creep is a thermally activated process, atomic diffusion becomes a significant factor and shows an exponential dependence on temperature. Therefore, the mobility of atoms or vacancies increases rapidly with temperature, atoms can diffuse through the lattice of the material. Because high thermal energy makes plastic deformation possible under lower stresses if sufficient time is provided. At a temperature substantially below 0.4Tm, the strain is virtually independent of time and creep becomes less-diffusion controlled (2,7).

Creep rate is also very sensitive to the applied stress level. At low stress and/or low temperature, some primary creep may occur but this falls to a negligible amount in the secondary stage when the creep curve

becomes almost horizontal. With the increase of applied stress and / or temperature, the rate of secondary creep increases, with further increase in stress, the primary and secondary stages are shortened or even eliminated, and the tertiary creep predominates leading to inevitable catastrophic failure (2,7).

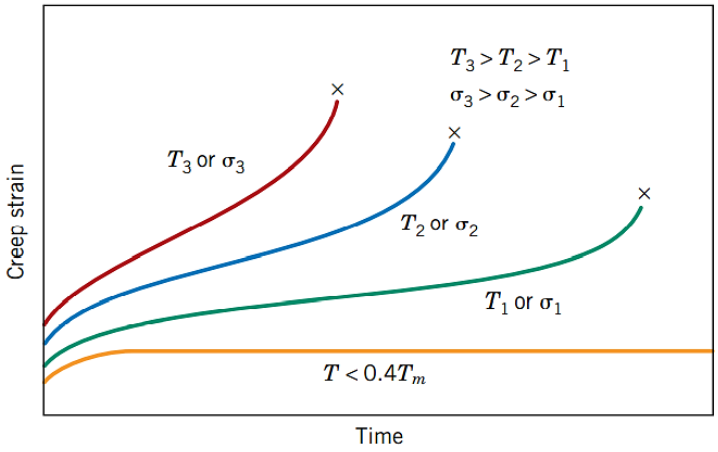

Fig.4: Effect of different stress (σ) *and temperature (T) on creep behavior.*

With either increasing stress or temperature, the following will be noted, figure4:

(1) The instantaneous strain at the time of stress application increases.

(2) The steady-state creep rate increases.

(3) The rupture lifetime decreases.

Most rate-dependent behavior in metals, such as creep is attributable to being a thermally activated process which in turn, depend on the stress, strain rate, deformation, and temperature. The strain rate at a given stress level is extremely sensitive to temperature (it goes much faster at high temperature). The higher the temperature, the more deformation and the more pronounced is the creep phenomena. Thus, creep is strongly temperature dependent, and a measurement of the temperature dependence of creep is important (6,8).

The rate at which deformation proceeds is described by an Arrhenius rate law equation:

$\epsilon = A_o \exp(-Q / RT)$

ϵ is steady-state creep rate or the tensile strain rate.

A_o is constant proportional to number of dislocations.

Q is the activation energy for dislocation motion (to free from obstacles).

R is gas constant and T is absolute temperature in Kelvin.

III.Mechanisms of creep in metals:

Creep deformation involves mechanisms at the atomic scale. Depending on the temperature range and the stress level, several theoretical mechanisms have been proposed to explain the different creep behavior of crystalline materials, these include (9):

1-Diffusional creep.

2-Dislocation creep that involves dislocation glide and climb.

3. Grain-boundary sliding.

1.**Diffusional creep**:

Diffusion creep represents a creep process controlled by diffusion of atoms or vacancies in the material, under low applied stress, where stresses not high enough to move dislocations (as the crystal resistance almost inhibits dislocation motion) but enough to help atomic diffusion by passive movement of atoms from higher concentration to lower concentration till equilibrium is the key mechanism for this type of creep deformation (5,10).

At low stress a high temperature is needed to cause a measurable creep rate, when the temperature range T > 0.4Tm, creep can be divided into two major groups, depending on the path of diffusion of vacancies: **boundary mechanisms**, in which grain boundaries diffusion takes place at moderately elevated temperatures (Coble creep) and **lattice mechanisms,** at high temperatures diffusion through the lattice becomes dominant and more rapid, so bulk diffusion takes place (Nabrro-Herring creep), figure 5 (5,10).

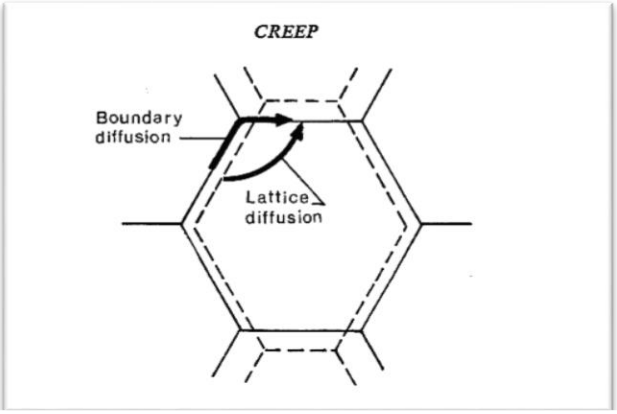

Fig.5: Diffusion Paths in a strained crystal at elevated temperature.

1.1. Nabarro-Herring creep

When a low stress is applied on a polycrystalline material at high temperature, diffusion of vacancies and atoms takes place through the crystal itself, the grain interiors by bulk diffusion because the energy needed for vacancy diffusion within the lattice is typically larger than that along the grain boundaries. As a tensile stress is applied to grain boundaries, the grain boundaries that are perpendicular to the stress, are in tension, distended, while the grain boundaries that are close to parallel to the tensile stress are in compression. Diffusion creep rate is a linear function of the applied stress, so stress alters the atomic volume in these regions; it is increased in regions experiencing a tensile stress and decreased in the volume under compression. Vacancies diffuse from grain boundaries that are under tensile stress (higher vacancy concentration) towards grain boundaries under compressive stress (lower vacancy concentration). Vacancy diffusion passes through the grain itself, where atoms can be considered to flow in the opposite direction. The atomic diffusion leads to elongation of the grains in the tensile direction, figure 6 (10).

1.2.Coble creep

Coble creep is based on diffusion along the grain boundaries instead of in the bulk. At low or moderately elevated temperature and low stress, the main diffusion path is via grain boundaries, because the energy needed for grain boundary diffusion is significantly lower than for diffusion through the bulk of the crystal and the cross-sectional area available for diffusion along grain boundaries is much less. Grain boundaries represent "easy paths" for diffusion since atoms at grain boundaries are less closely packed, disordered than in a perfect lattice, diffusion of atoms or vacancies is more rapid and easier through the porous grain boundaries. The atomic diffusion in the lattice becomes progressively more difficult and slows down relative to grain boundary diffusion with decreasing temperature, figure 6 (9,10).

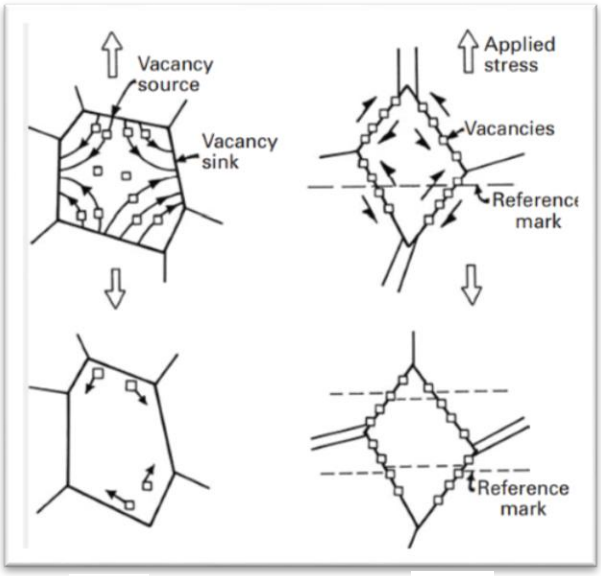

Fig.6: Flow of vacancies according to (a) Nabarro-Herring c and (b) Coble mechanisms resulting in an increase in the length of the specimen.

2.Dislocation creep:

Dislocation creep is a deformation mechanism in crystalline materials, which involves the movement of dislocations through the crystal lattice of the material causing plastic deformation. It is the dominant deformation mechanism in most crystalline materials. Dislocation creep occurs through dislocation glide and dislocation climb (12).

2.1.Dislocation glide:

Dislocation gliding is the normal plastic deformation movement along the slip planes. In metals, it involves motion of dislocation which is controlled by glide at low temperatures and does not depend on diffusion. Dislocation motion may be stopped and obstructed by obstacles on its slip plane, such as other dislocations, precipitates, grain boundaries which exert forces on a dislocation as it moves on its slip plan and increases the resistance to dislocation movement. Any form of obstacle used for blocking dislocations

would then reduce creep deformation. At low applied stress, dislocations are unable to bow around or cut through the obstacle. it's not enough for moving dislocation to overcome the obstacle via dislocation slip alone (9,10).

2.2 Dislocation climb:

At elevated temperatures, the increased energy permits dislocations in a metallic material to climb to a different plane. In climb, the atoms gain energy, so atoms move either to or from the dislocation line by diffusion (diffusion of vacancies or interstitial atoms through a crystal lattice), causing the dislocation to move in a direction that is perpendicular to the direction of slip plane. The dislocation, then escapes from lattice imperfections and overcome those obstacles, continues to slip, glide on the new plane, causing additional deformation of the specimen even at low applied stresses, figure 7 (9,10).

This process repeats itself each time when the dislocation glides, along new slip plane until it encounters another resisting obstacle, in which atoms move out of the slip plane, then the dislocation again climbs up or down to another slip plane and the process is repeated**.** Thus, dislocation creep involves the sequential processes of dislocation glide coupled with dislocation climb that assists to overcome barriers by a process of diffusion motion of vacancies(10,11).

Dislocation gliding produces almost all the creep strain, which is much faster than dislocation climb that controls the creep rate (how rapidly the dislocations can overcome obstacles that obstruct their motion by the slower atomic diffusion and mobility of vacancy) (12).

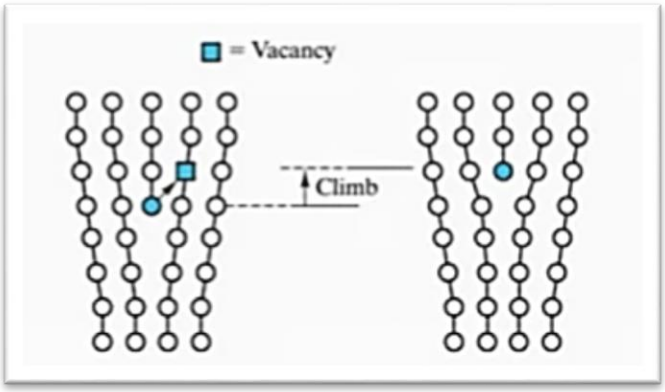

Fig.7: Dislocations can climb when atoms leave the dislocation line to fill vacancies.

3.Grain boundary sliding (GBS):

The onset of tertiary creep stage is a sign that structural damage has occurred in an alloy. when occurring at sufficiently high temperature, grain-boundary sliding usually plays an important role in this stage. Large amounts of grain boundary sliding may occur, under the action of shear stresses acting on the boundaries, causing the movement of grains relative to each other and leading to initiation and propagation of inter-crystalline cracks, voids formation, and ultimately fracture (9,10).

Grain-boundary sliding does not represent an independent deformation mechanism. The sliding of the grain boundaries, under the influence of the applied shear stress, and diffusional creep can be considered to take place sequentially in the individual grain. Diffusional creep leads to grain separation,

which is followed by grain-boundary sliding causing to 'heal' voids between grain, that would otherwise open up due to grain boundary diffusion. To maintain grain continuity and prevent the formation of internal voids or cracks during diffusional process, the grain-boundary sliding rate must exactly balance the diffusional creep rate, figure 8 (9,10).

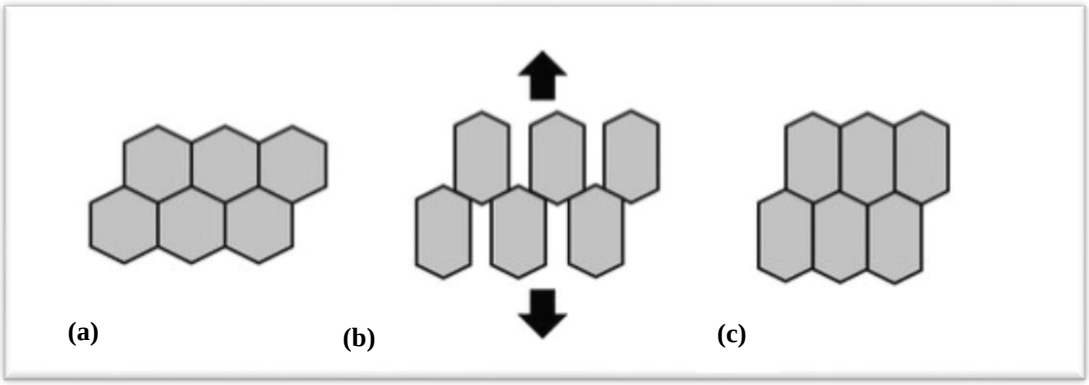

Fig.8:

a) Initial configuration of six grains before creep deformation

b) Following diffusional creep, under tensile load applied, one dimension of the grains is increased and the other decreased creating gaps, voids between the grains.

IV.Effect of grain size on creep of metals:

Several factors affect the creep characteristics of metals. These include melting temperature, elastic modulus, and grain size. In general, the higher the melting temperature. The higher the metal exposed to high temperatures, the larger or coarser the grain size, the better a material's resistance to creep than refined grains so that the fracture time increases giving it an advantage over the creep properties of metals (2,10).

The effect of grain size on secondary or steady-state creep rate has been studied to a great extent. The creep mechanism of metals can occur in grain boundary sliding (GBS), diffusion creep (Nabarro–Hearring diffusion creep and Coble creep), and dislocation creep. The mechanism is theoretically equally influenced by grain size that steady-state creep rate increases with increasing grain diameter (13).

The grain size of polycrystalline metals is important since the amount of grain boundary surface has a significant effect on many properties of metals, especially strength. Grain boundaries at lower temperatures usually strengthen polycrystalline metals by providing barriers to dislocation movement. A fine-grained material is harder and stronger than one that is coarse grained because the former has a greater total grain boundary area to impede, stop dislocation motion. However, during creep deformation at elevated temperatures, grain boundary sliding may occur, and the grain boundaries become regions of weakness (grains shear relative to each other at grain boundaries, where large amount of strain is believed to be accumulated by the sliding of individual grains relative to each other). The contribution of grain-boundary

sliding to plastic deformation is more significant the greater the grain boundary surface per unit volume. Since the grain-boundary surface is inversely proportional to the grain size, fine-grained material permits more grain boundary sliding, resulting in higher creep rates than in materials with coarse grain sizes (13,14).

Also, the grain size plays a major role in diffusional creep, where creep rates increase linearly with the stress and inversely with the square of grain size. As grain size decreases, the area of the grain boundaries increases, the creep rate increases, the length of the diffusion path is smaller, and diffusion is faster than for coarser-grained ones. A practical way of having an alloy with high resistance to Nabarro-Herring or Coble creep is to increase the size of the grains, by coarse grains. As well creep resistance is improved if diffusion rates are reduced, diffusion is lower as well in materials with high melting point (5).

High-temperature creep is dependent on dislocation climb, the creep rate increases with increase in the rate of diffusion of vacancy to the dislocation. Vacancy can diffuse more rapidly along high-energy grain boundaries than through the interior of the grains. Vacancy diffusion is rapid in a fine-grain-size material having a greater number of grain boundaries and so, the creep rate is higher. While material with coarser grain will have lesser grain boundary areas for which vacancy diffusion is relatively slow, the material will result in a lower creep rate and higher resistance to creep (5).

Creep rates are also reduced by utilizing materials with high elastic modulus, the greater the elastic modulus (the greater the stiffness of the material which depends on the strength of the bond), the less is the strain rate. Thus, the dislocation creep barriers or obstacles in higher elastic moduli materials take longer time to overcome and thereby the slower creep rates and the better the creep resistance (13).

V. Dental examples of creep:

Dental amalgam is a good example of a material showing creep behavior. Creep of amalgam is dependent on the yield strength of the material and the temperature of the environment. It only becomes a serious problem when the environmental temperature is greater than half the melting temperature, where the amalgam phases have very low melting temperatures, slightly above the room temperature (about 80°C). As well when the restorations are subjected to stresses of mastication, which are usually well below the normal static yield strength, and for an extended period. Creep will be occurring and produce continuing plastic deformation of the restoration, the process can, over time, be very destructive to a dental amalgam filling causing the amalgam to extend out of the restoration site, increasing its susceptibility to marginal breakdown (15).

Low-copper dental amalgam with mercury-based phases, silver-mercury $\gamma 1$(Ag_2Hg_3) and tin-mercury $\gamma 2$ (Sn_8Hg) phases are most prone to creep. When an amalgam creeps, it is $\gamma 1$ phase that deforms plastically, it has a big effect on creep rates and $\gamma 2$ phase increases the creep rate. The mechanism of creep in dental amalgam is grain boundary sliding, where the presence of $\gamma 2$ phase at the grain boundaries accommodates the sliding of the $\gamma 1$ grains, giving rise to higher creep values. Increased creep rate is shown by larger $\gamma 1$ volume fractions, decreased creep rate is shown by larger $\gamma 1$ grain sizes. Thus, for a given load at a given time, the low-copper amalgam has a greater strain (1,16).

High-copper amalgam have lower creep values prevailing because γ2 phase has been eliminated and copper-tin η (Cu6Sn5) crystals act as barriers to deformation on γ1 grains blocking grain boundary sliding of γ1 and therefore are responsible for decreased creep values of high copper alloys (1,16).

Low-copper amalgam shows greater strain, and higher amount of creep than high copper amalgam, figure 9. The clinical importance, is the greater creep in low-copper amalgam results in more amalgam protrudes at the margin of the restoration and greater marginal overhanging and fracture, leaving a ditched amalgam around the margin which can lead to secondary decay. This contributed to its decline in popularity, low-copper amalgam is no longer commonly used in dentistry. While the absence of the corrosion-susceptible γ2 phase in the microstructure of high-copper amalgams is assumed to be the principal factor responsible for the superior resistance of these alloys to marginal breakdown. A correlation between creep and marginal breakdown exists, where amalgam alloys having creep values below 1%, were free of γ2 phase and show differences in clinical performance. Whereas amalgam having creep values higher than 1%, were found to contain γ2 shows marginal breakdown (16).

Thus, the primary importance of creep is to determine the presence and absence of tin-mercury (γ2) phase and predict the clinical performance of amalgam restorations. this was subsequently adopted as one of the prime tests in both the American Dental Association (ADA) and the FDI World Dental Federation (FDI) specifications (16).

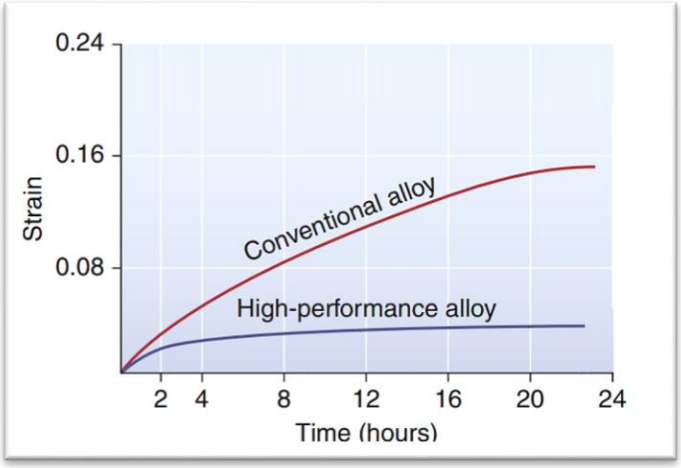

Fig.9: Creep curves for conventional (low-copper) and high-performance (high-copper) amalgams.

To test creep of amalgam, according to the ADA specification number 1 for dental amalgam published in 1976 and revised in 1979. Creep test conducted on specimens, where the axial length of each specimen shall be measured and recorded as original length. The specimens shall be stored at 37± 3oC for seven days. A stress of 36 MPa shall be applied continuously to the specimen for not less than four hours at 37±3°C. The change in length between the one-hour and four-hour readings shall be recorded and the creep shall be computed as follows: creep (%) equals length change between one and four hours divided by original length multiplied by 100. The average of the creep for the specimens shall be recorded to the nearest 0.1%. the acceptable creep value in a dental amalgam should be less than 3% (17).

Sag is the permanent deformation potential of long-span metal bridge structures at porcelain-firing temperatures under the influence of the mass of the prosthesis. Sag resistance is the ability of a dental alloy to

resist deformation under its own weight during porcelain-firing and soldering. It is particularly important in long-span bridges, where due to increased weight of the prosthesis, the porcelain-firing temperatures may cause the unsupported alloy substructure to deform permanently, distortion of the framework of long span bridges during the firing process may occur, which results in an ill-fitting restoration. Therefore, the 'sag' phenomenon affects the metallic substructure and is of vital importance to the overall fit of ceramo-metal restorations (1).

Metals used in dentistry for indirect restorations for porcelain veneers have melting temperatures that are much higher than mouth temperatures, thus, they are not susceptible to creep deformation intraorally. As well, should be compatible with porcelain veneering, having their melting temperature significantly higher than the firing temperature of the porcelain. The metal framework must not melt during porcelain firing and must resist high temperature "sag" deformation (1).

Some alloys used for metal-ceramic prostheses can sage at porcelain veneering temperatures. Earlier gold alloys were used for ceramo-metal restorations, these alloys had certain disadvantages like low modulus of elasticity and poor sag resistance during the porcelain firing cycle. The highest sag rate was found with high gold alloys (gold-platinum pallidum alloys), whereas gold-palladium and palladium-silver based alloys had lower rates. Due to sagging caused by thermal creep of the alloy, distortion of the framework of long span bridges during the firing process may occur, leading to an inaccurate fit of the restoration (18).

Base metal alloys have substituted the use of gold alloys by having higher hardness and greater rigidity. This allowed the fabrication of long span with lesser thickness, enabling the coping to reach 0.1 to 0.2 mm thick. Moreover, higher melting range reduces the risk of distortion and sagging of metal substructure during porcelain firing which led to use of base metal alloys for fixed restorations, these materials are far more stable at porcelain firing temperatures than the gold-based alloys due to their superior sag resistance. Most of the non-precious alloys used are based on nickel chromium and cobalt chromium (18).

References:

1- Anusavice, K.J., Shen, C. and Rawls, H.R. (2012). Phillips Science of Dental Materials, 12th edition, Saunders, Philadelphia.
2- Callister WD, Rethwisch DG. (2009). D. Materials science and engineering.: An introduction. (Eight edition) Wiley, USA.
3- Pascoe KJ. (1978). An introduction to the properties of engineering materials (third edition). Van Nostrand Reinhold (UK) Co. LTD.
4- Smith, W. F. William F., Hashemi, J., & Presuel-Moreno, F. (2019). Foundations of materials science and engineering. Sixth edition. New York, Mc-Graw Hill.
5- Amit Bhaduri (2018). Mechanical Properties and Working of Metals and Alloys, Springer
6- Alan M. Russell, Kok Loong Lee. (2005). Structure-Property Relations in Nonferrous Metals, Wiley, Hoboken, New Jersey.
7- J. Li and A. Dasgupta, (Sept. 1993). Failure-mechanism models for creep and creep rupture, in IEEE Transactions on Reliability, vol. 42, no. 3, pp. 339-353.
8- McLean, D. (1966). The physics of high temperature creep in metals. Reports on Progress in Physics, 29(1), 1–33.
9- Askeland DR, Fulay PP. (2009). Essentials of Materials Science and Engineering. Second Edi.; 2009. http://library1.nida.ac.th/termpaper6/sd/2554/19755.pdf.
10- Thomas. H. Courtney. Mechanical Behavior of Materials. McGraw-Hill Publ. Co., Singapore 2000. Waveland Press. USA.
11- Yang, H., Gavras, S., & Dieringa, H. (2021). Creep Characteristics of Metal Matrix Composites. Encyclopedia of Materials: Composites, 375–388.
12- Salma K. Rizk and Reem A. Hany. Failure of metals and alloys in dentistry. Biomat. J., 1 (7),27 – 36 (2022). https://doi.org/10.5281/znodo.5829408.
13- Smith, W. F. (William F., Hashemi, J., & Presuel-Moreno, F. Foundations of materials science and engineering. Sixth edition. New York, Mc-Graw Hill. 2019. P.92-182.
14- Anwar, Mochammad & Widjaya, Robert & Prasetya, Leonardo & Arfi, Abdul & Mabruri, Efendi & Siradj, Eddy. (2022). Effect of Grain Size on Mechanical and Creep Rupture Properties of 253 MA Austenitic Stainless Steel. Metals. 12. 820. 10.3390/met12050820.
15- Van Noort R, Michele B., 2013. Introduction to Dental Materials (fourth edition). Elsevier Health Sciences. p. 7-10. 5. Lawn B. Fracture of Brittle Solids - second edition. Science Series. 1993.
16- Greig, Vicki. (2012). Craig's restorative dental materials, 13th edition. British dental journal. 213. 90. 10.1038/sj.bdj.2012.659.
17- Revised American Dental Association Specification No. 1 for Alloy for Dental Amalgam. (1977). The Journal of the American Dental Association, 95(3), 614–617. doi: 10.14219/jada.archive.1977.0123.
18- Prakash, P., D'Souza, D., Kumar, M., & Viswambaran, M. (2012). Effect of firing cycle and surface finishing on the sag resistance of long-span metal ceramic framework using base metal alloys—an in vitro study. Medical Journal Armed Forces India, 68(2), 145–150. doi:10.1016/s0377-1237(12)60016-1

Biomaterials Journal
http://www.biomatj.com
Online ISSN: 2812-5045

Type of the Paper (Review Article)

Thermal Analysis of Dental Materials : A Review

Sherine Sherif Stino [1,*]

[1] Assistant lecturer, Biomaterial Department,Faculty of Dentistry, Cairo University
* Corresponding author e-mail: sherine.stino@dentistry.cu.edu.eg

Citation: *Sherine Sherif Stino .Thermal Analysis of Dental Materials : A Review . Biomat. J., 2 (1),13 – 23 (2023).*

https://doi.org/10.5281/znodo.5829408

Received: 25 December 2022
Accepted: 15 January 2023
Published: 31 January 2023

Abstract: The mostly used TA techniques for materials characterization are differential thermal analysis (DTA), differential scanning calorimetry (DSC) and thermogravimetric analysis (TGA). TGA is mainly used to examine the decomposition of materials by monitoring mass change with temperature. DTA and DSC are widely used for examining the phase changes of materials, where DTA measures temperature difference and DSC measures heat difference.

Keywords: : *Thermal analysis; DTA; TGA; DSC.*

Thermal analysis (TA) is a group of analytical techniques that measure properties or property changes of materials as a function of temperature. These techniques are mainly applied for the characterization and investigation of structure decomposition, thermal stability, and phase transition. Many TA methods have been developed for a variety of examination purposes and are distinguished from one another by the property they measure. The mostly used TA techniques for materials characterization are differential thermal analysis (DTA), differential scanning calorimetry (DSC) and thermogravimetric analysis (TGA). TGA is mainly used to examine the decomposition of materials by moni-toring mass change with temperature. DTA and DSC are widely used for examining the phase changes of materials, where DTA measures temperature difference and DSC measures heat difference. The term differential is used since changes in a specimen are measured with respect to a standard reference material (1).

1.Differential Thermal Analysis (DTA)

Differential thermal analysis measures the temperature difference of the sample under investigation and a thermally inert material (generally alumina) known as the ref-erence against time or temperature. This temperature difference is then recorded while the sample and the reference are subjected to a controlled identical temperature pro-gram (heated or cooled) in an environment at a controlled uniform rate (same heat flow) (1).

1.1 Principle of DTA:

As the sample is heated, it undergoes reactions and phase changes it can be de-tected relative to the inert reference, energy is emitted or absorbed, and a temperature difference is detected between the reference and the sample. The temperature differ-ence between sample and reference (ΔT) should be zero when no thermal event or re-action occurs in the sample, because of similar thermal conductivity and heat capacity between the sample and reference. But when the sample undergoes thermal event such as physical or chemical changes, ΔT will be generated and becomes different. When there is a physical change in the sample then heat is absorbed or released. For endothermic reaction, such as melting, dehydration, vaporization, loss of water or solvent the heat (energy) is absorbed and the temperature

of the sample is decreased, so the sample would be at a lower temperature than that of the reference. While an Exothermic reac-tion, as crystallization, oxidation, polymerization the heat is released, and the sample temperature would be higher than the reference. These temperature differences be-tween sample and reference produces a net signal, which is then recorded. A plot of the temperature difference reveals exothermic and endothermic reactions that may occur in the sample (2).

1.2 Sample presentation:

Almost any physical from of sample can be accommodated such as solid (amor-phous or crystalline), liquid or gel, using various sample crucibles made from different materials (e.g.: platinum, aluminium). Sample size is usually small, a typical optimum sample weight of 50-100 mg (3).

1.3 Instrumentation:

DTA instrument is composed of fundamental components, figure 1. The sample is first loaded into a container and placed onto the sample pan or crucible (e.g., metallic or ceramic), figure 1. An equal quantity of inert material is placed in another container onto the reference pan. The dimensions of the pans should be nearly identical to be heated at a uniform rate. The sample and the reference weights must be equal, holders arranged symmetrically within a single heat source furnace and subjected to a common temperature program. The furnace and the holders are enclosed by an insulat-ing material. As well, there is an electronic temperature regulator, programmer to ensure a constant rate of heating, and thermocouples for temperature regulation which are usu-ally inserted into holders. The temperature difference between the sample and the ref-erence are measured by the two thermocouples coupled in contact with the sample and with reference substance.The thermocouples are attached to an amplifier which con-verts the heat signal into an electrical signal and send the differential thermocouple out-come to the computer device to display in the form of a DTA curve or thermogram. The signal is only produced if a temperature deviation is observed; if the sample doesn't un-dergo any reaction, no signal is generated as no temperature difference is observed (4).

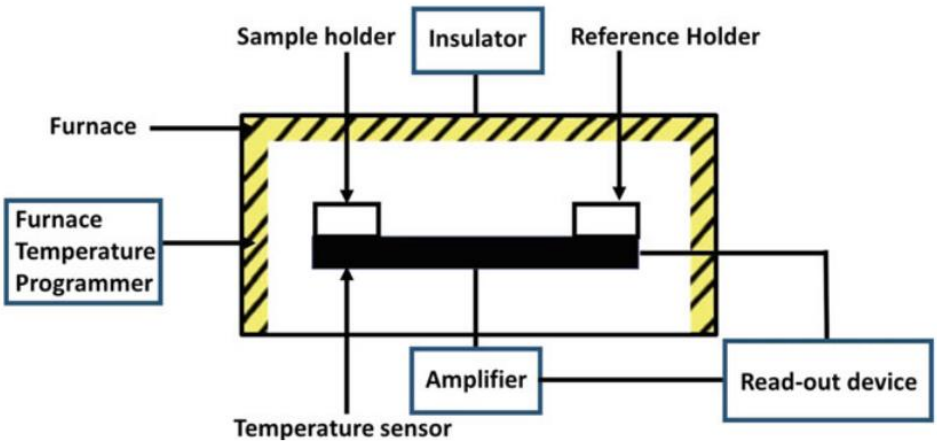

Figure 1: Schematic representation of fundamental components of DTA

Characteristics of DTA Curve:

The temperature difference of a sample when heating or cooling are shown in a DTA curve or thermogram, figure 2. DTA curve is a plot between differential temper-ature (ΔT) and temperature of reference (T). DTA curve may be endothermic (downward plot) or exothermic (upward plot) (2). A downward plot is endothermic, DTA curve demonstrate that the sample temper-ature is less than that of the reference material, whereas an exothermic reaction is rep-resented as an upward plot where the specimen temperature is greater than that of the reference. This temperature difference betweensample and reference produces a net signal, which is then recorded. if there is no reaction happening in the sample material, then

the sample temperature remains the same as that of the reference material (2).A DTA curve can be affected by various factors. These could be either physical factors such as adsorption, crystallization, melting, and vaporization or chemical factors such as oxidation and reduction. It can also be affected by the characteristics of the sam-ple, such as amount, shrinkage, particle size, or instrumental factors such as the record-ing system sensitivity.

1.4 Interpretation of DTA thermograph (2):

-Line AB: no reaction in the sample material, value of ΔT is zero.
-Point B: initial temperature point, the curve rises from the baseline due to the exo- thermic reaction and it forms a peak BCD.
-Point C: the process of heat is completed. Maximum temperature peak or heat value. The peak temperature is the characteristic of the sample ma terial.
-Point D: Heat is decreased up to D point, final temperature.
-BCD area under peak has a direct relation with the amount of reacting material, and this amount can be determined by comparing the area of a characteristic peak of the sample with areas from a series of standard known samples analyzed under identical conditions.

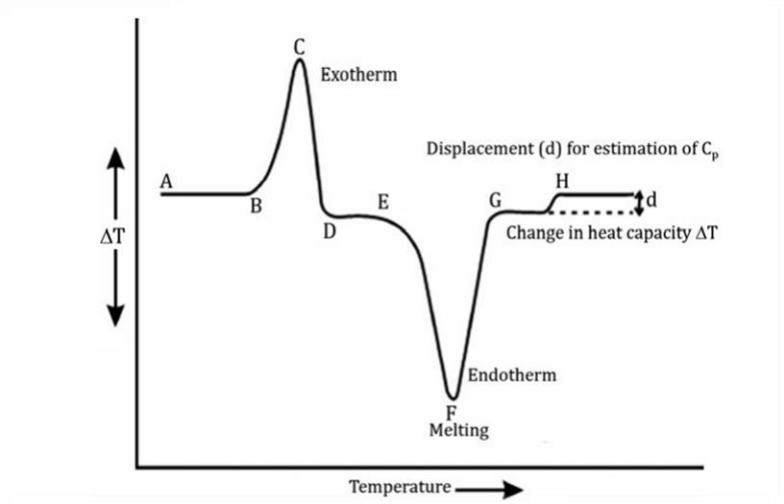

Figure 2: Characteristics of DTA curve

1.5Advantages (2,4):

1.Simple, Ease of use and adaptability.
2.Small sample size (tenth of a gram order), this allows the temperature to be homogeneous in the whole sample, avoiding a temperature difference along the sample thatmay affect results.
3.Both exothermic and endothermic reactions can be determined accurately.
4.DTA apparatus can operate over a wide temperature range, from −150 to 2400°C, using various heating and cooling programs. DTA feature is important for examining materials with high melting temperature such as ceramics and some metals.

1.6 Disadvantage (2,4):

1.Difficult to quantitatively obtain mass change during the test.
2.Complicated determination of phase transformation temperatures.
3.Low sensitivity and accuracy in quantity measurements of thermal analysis, when the absorbed or released heat during the measurements is not enough (too low) to be recognized; thus, the peaks associated with these thermal processes are not ap-preciated or are missed in the DTA curve.

4.Inherent limitation for its the development into a technique of high precision: The assumption of a constant value of the heat capacity of the sample and the assump-tion that the sample temperature is uniform at each time instant.

1.7 Applications (2,4):

1.Used to study the characteristics of materials, especially polymers it is based on measurement of properties like, melting point, decomposition temperature, crystal-lization and degree of polymerization can be assessed.
2.To distinguish exothermic and endothermic processes.
3.Qualitative identifications of material can be done by comparing the DTA of sample to DTA thermal curves of know materials.4.DTA is widely used in the pharmaceutical and food industries.

2.Differential scanning calorimetry (DSC)

Differential Scanning Calorimetry (DSC) is a thermal analysis method which measures the difference in the amount of heat or the heat flow rate (ΔH) between the sample and an inert reference as a function of time or temperature, while both are subjected to a controlled temperature program. DSC measures the energy required to keep both the reference and the sample at the same temperature (3).

DSC differs fundamentally from DTA in that the sample and the reference are both maintained at the temperature predetermined by the program. DSC is a calorimetric method, where heat flow (uptake or release) and energy differences are quantitatively measured. While in DTA, the temperature of the sample is monitored with respect to a reference sample, DTA is a qualitative technique which measures temperature differences and do not provide any quantitative data for energy (5).

2.1 Sample presentation:

Samples are typically solid, can be in powder form such as metals, ceramics, organic and inorganic materials and predominately polymers. Liquid samples can also be tested. Sample size is very small, the sample weight in DSC experiments is in the range of 5 to 20 milligrams [6]. For sample and reference crucible, A variety of sample pans or crucibles are available in different materials to handle different kind of samples measurements according to the material used to study, figure 3 (7). **The standard aluminum sample pans** can be used for solids and powders that do not decompose or boil in the range of -170° to 600 °C. They are used with most routine applications, can also be used for nonvolatile solid samples such as metals, and polymer and inorganic materials provided that they do not react with aluminum. **Platinum, copper, gold or alumina pans** are used for samples which react with aluminum (e.g., biological samples).
Also, they are used where high internal pressures are required or when sample of interest has a transition in high temperatures region (600-725°C), particularly useful in the specific heat capacity determination of liquids. In cases of undesirable metal-sample interactions occur, graphite pans are the method of choice(7).

Figure 3: Sample pans used for DSC testing

2.2 Principle of DSC:

The basic principle of DSC, it studies what is the effect of heating on the sam-ples. It measures the heat flow related to the thermal transitions in materials, as a func-tion of time and temperature. Any event, such as loss of solvent, phase transitions, crys-tallization temperature, melting point, glass transition temperature of the sample, re-sults in a change in its temperature. Thus, it provides qualitative and quantitative infor-mation about physical and chemical changes that involve endothermic (heat flow into sample), exothermic (heat flow out of the sample) processes or changesin heat capacity. The available DSC systems have a wide range of temperature capability, from -60 ^{O}C to >1500 ^{O}C (3).

2.3 Instrumentation:

DSC device may be one of two types: heat-flux DSC or power compensation DSC, the main difference is being mainly ontheir instrumentation design, depending on the principle of measurement used. The sample is placed in a crucible or a pan, then inserted in the cell of the machine, while the reference pan is empty. It's in this cell where the test is conducted, and the data is collected. Having extra material in sample pan means that it will take more heat to keep the temperature of the sample pan increasing at the same rate as the reference pan (8,9).

2.3.1 Heat-Flux DSC is also called ''quantitative DTA'' as it measures the tempera-ture difference directly and then converts it to a heat-flow, energy difference. The sam-ple and reference are interconnected by a metal disk and placed in a single furnace, fig-ure 3a. As the furnace is heated at a linear heating rate, the heat is transmitted to the sample and reference pan through the metal disk. The difference of the temperature between sample and reference is due to the changes of heat capacity (Cp) of the sam-ple (the empty reference side heats faster than the sample side during heating of the DSC cell, so the refer-ence temperature increases a bit faster than the sample temperature). This temperature difference creates the heat flow signal and is measured as a function of heat(1,3).

2.3.2 Power-compensated DSC belongs to class of heat-compensating calorimeters. The heat to be meas-ured is compensated with electric energy by increasing or decreasing an adjustable Joule's heat. The sample and reference are placed in separate furnaces, where their temperatures are controlled and heated, by sep-arate temperature control-lers, and both have the same temperature figure 3b. As soon as changes in the sample occur, extra (for an endothermic effect) or less (for an exothermic effect), temperature differences between the sample and reference are compensated for by varying the heat required to keep both pans at the same temperature. The difference in power electrical input supplied to the sample and to the reference, to keep their temperatures as nearly the same as possible (the energy which is required to obtain zero temperature difference between sample and reference) is measured throughout the entire analysis. The energy difference is plotted as function of sample temperature (3,9).

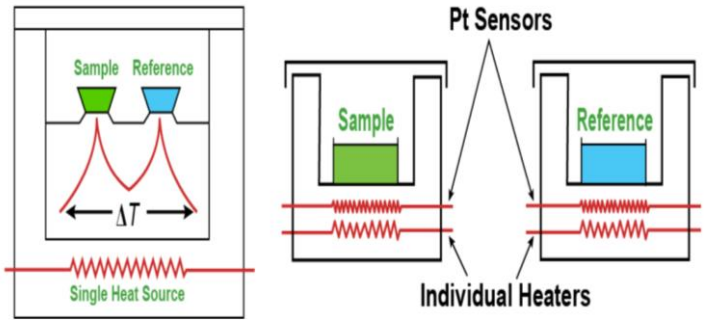

Figure 4: Schematic representation of Heat Flux DSC (a) and Power Compensated DSC (b)

2.4 Interpretation of DSC Curve:

The result of a DSC experiment is displayed in the form of a DSC thermograph, or a curve in which heat flow is plotted versus sample's temperature. Concerning interpreta-tion of DSC thermographs, The following phenomena are the most common obtained from a DSC experiment, no onesample would contain all the transitions shown in figure 4 (10).

(i)Glass transition temperature (Tg) which is the most common measured tran-sition by means of thermal analysis techniques.

(ii)Crystallization (Tc), appearing as a well-defined exothermic process.

(iii)Melting of the specimen (Tm). Well-defined endothermic peak, since energy must be absorbed by the sample to get melted.

(iv)Heat of fusion H which is determined by integrating the peak area.

(v)Cure reactions appearing as shallow and broad exotherms.

(vi)Moisture loss appearing as shallow and broad endotherms.

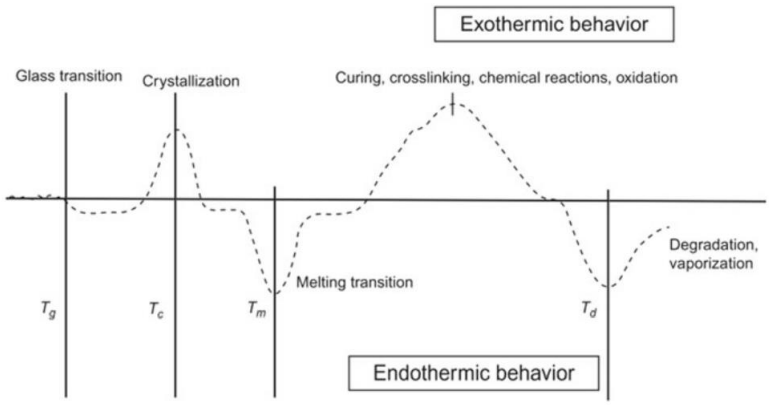

Figure 5: Schematic illustration of main events detected by DSC in a polymer

On heating a polymer to a certain temperature, plot will shift a step downwards, there is more heat flow, where an increase in the heat capacity of the polymer occurs. This change in heat capacity that occurs at the glass transition, help to use DSC to measure a polymers glass transition temperature. After glass transition, the polymers have a lot of mobility, when they reach the right temperature, they will give off enough energy to move into ordered arrangements, the temperature at the highest point in the peak is usually considered to be polymer's crystallization temperature. If we heat polymer past its Tc, eventually another thermal transition will be reached, called melting Tm. When its reached, the polymers crystals begin to fall apart that is they melt. This means that the little heater under the sample pan must put a lot of heat into the polymer, to both melt crystals and keep the temperature rising at the same rate as that of reference pan. this extra heat flow during melting shows up as a big dip endothermic peak on DSC plot, figure 4 (11).

2.5 Advantages (2,4):

1. DSC is the most employed thermal analytical technique by the research community due to its low price, efficiency of handling and its relatively fast.
2. DSC is widely used to get information about glass transition temperature (Tg), melting point (Tm), crystallization temperature (Tc), the heat of crystallization (Hc), the heat of melting and heat absorbed or evolved during the cure reactions or decomposition reactions (9).
3. A very small amount of sample can be used and the sample present in any form can be tested in this technique.
4. A wide range of temperature control is possible.

5. It can be used for studying many types of chemical reactions.

2.6 Disadvantages (2,4):

1. Inability to distinguish between samples having their thermal processes occur in the same temperature ranges (same melting points or glass transitions), the interpretation of the data becomes difficult due to overlapping of the peaks of phase transitions in the thermogram.
2. Interpretation of result is very difficult. It is highly dependent upon analyst experience. Subtle changes require detailed knowledge of chemistry and material information to understand.
3. The accuracy of the results decreases when trying to analyze nanomaterials or complex thermal processes.
4. DSC technique is sensitive to the heat-flow changes and the instrument calculates them as an average of multiple readouts. Using low heating rates or large quantities of samples could prevent this.

2.7 Applications (1,2,8):

1. Characterization of various kinds of samples for many applications can be done like polymers, pharmaceuticals, foods/biologicals, organic and inorganics chemicals and ceramics.
2. Material Identification: one of the primary uses of DSC, as to know if a polymer is semi crystalline or amorphous.
3. Phase transitions: determination of melting and crystallization points as well as phase transitions by measurement of the change of energy over temperature. DSC is widely used for examining polymeric materials to determine their thermal transitions. Important thermal transitions include the glass transition temperature (Tg), crystallization temperature (Tc), and melting temperature (Tm) as well as determining special properties of polymers such as crystallinity, curing status, polymer content, and stability. 4. Determination of Phase transformation and phase diagrams: the curve peaks of DSC reveal solid-state phase transformations over a temperature range.

3.Thermogravimetric Analysis (TGA)

Thermogravimetric analysis is a technique in which the mass of a substance is mon-itored as a function of temperature or time as a sample is subjected to a controlled tem-perature program in a controlled atmosphere. It measures the change in weight of the sample during the process of heating or cooling. It is used to measure the phase changes, glass transition, and melting point. TGA is a powerful technique for the measurement of thermal stability of materials including polymers(4).

3.1 Sample presentation:

The sample pans (ceramic or platinum) can accommodate liquids, powders, films, solids, or crystal. The sample weight influences the accuracy of weight loss measure-ments, weight of the sample is up to 1g, typical sample is in mg, up to 50 mg of material is desirable in most applications and for volatile materials its around 20-100 mg of sample (12).

3.2 Principle of TGA:

TGA determines the amount and the rate of weight change of a substance with re-spect to temperature or time in controlled programmed conditions. The mass change profile (mass loss or mass gain) is continuously monitored and recorded as the sample is subjected to a controlled heating or cooling environment. TGA is used principally in the research and development of various materials to obtain knowledge and examine the strength of the material at a given temperature (thermal stability) as well as their com-positional properties (e.g., fillers, polymer resin, solvents). Additionally, it is used to un-derstand certain thermal events such as absorption, evaporation, decomposition, oxida-tion, and reduction, such events could bring drastic change in the mass of the sample.

3.3 Instrumentation:

TGA is conducted on an instrument referred to as a thermogravimetric analyzer, where mass, temperature, and time are considered its basic measurements. A thermo-gravimetric analyzer continuously measures mass while the temperature of a sample is changed over time. The fundamental instrument needed for TGA is a precision balance "Thermobalance" witha furnace designed to linearly increase temperature over time, which is regarded as the heart of a TGA unit (13). Main components of TGA apparatus:1.Highly sensitive scale, microbalance to measure weight change. The balance is located above the furnaceand is thermally isolated from any thermal effects, to max-imize the sensitivity, accuracy, and precision of weighing.2.Sample holder or crucible could be made from platinum, aluminum or ce-ramic, it is necessary that the crucible should possess at least 100^0C higher thermal sta-bility compared to experimental temperature conditions. The crucible holds the sample supported by the precision balance and located inside a programmable furnace.

Main components of TGA apparatus:

1. Highly sensitive scale, microbalance to measure weight change. The balance is located above the furnace and is thermally isolated from any thermal effects, to maximize the sensitivity, accuracy, and precision of weighing.
2. Sample holder or crucible could be made from platinum, aluminum or ceramic, it is necessary that the crucible should possess at least 100^0C higher thermal stability compared to experimental temperature conditions. The crucible holds the sample supported by the precision balance and located inside a programmable furnace. Furnace with temperature programming facility, that is heated or cooled during the experiment, to control the temperature of the sample. The furnace can scan over a wide range of temperature 25 – 1200 ^{0}C and it is constructed of quartz. The balance and the furnace assembly are the two key components of thermobalance.
4. Facility to supply the gas, for providing inert atmosphere or oxidizing environment and an infrared spectrometer added to TGA allows identification of gases generated by the degradation of the sample.
5. Computer for observing the weight and temperature changes, where the balance is calibrated in a manner that a change in weight of the sample produces a proportional electrical signal. The computer collects, stores this electrical signal and converts it into weight or weight loss, which is then plotted on the thermal curve and calculate the weight-loss fraction or percentage.

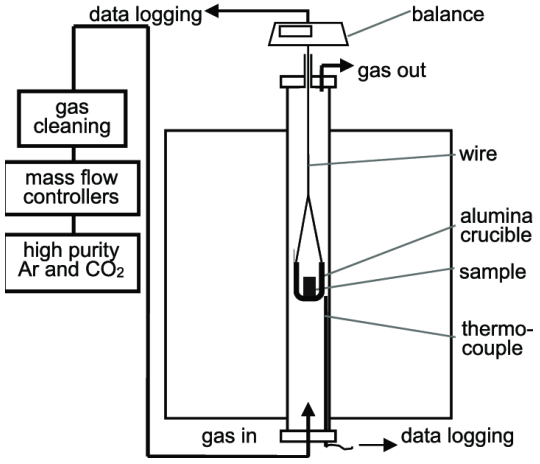

Figure 6: Schematic representation of components of TGA

3.4 Interpretation of TG curve:

Data are obtained by plotting a graph between the mass change as a function of the temperature or time and are interpreted from TGA curve or thermogram, figure 7. This example of TG curve exhibits a single stage of decomposition.

In the curve, **"Ti is the Initial Decomposition Temperature"** represents the temperature at which the onset of decomposition is initiated and point at which the weight change attains a magnitude that can be detectable by a thermobalance. **"Tf is the final decomposition temperature"** represents the temperature at which the decomposition reaction is completed and the point at which the weight change attains a maximum and cannot change further. The values of Ti and Tf depend on the thermal stability of the sampling analyzed. The temperature at which no weight loss takes place indicates stability of the material (13).

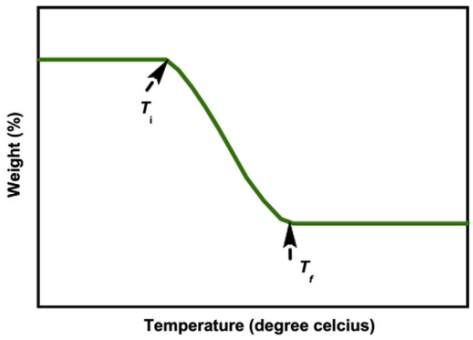

Figure 7: Typical thermogravimetry curve

The TGA curve is classified into the following seven different types based on their shapes, figure 8 (13).

Type i: No mass change over the entire temperature range used for analysis; the sample is considered stable. It may be because the thermal stability of the sample is higher than the temperature range of the sample.

Type ii: There is a mass loss region, which is then followed by a constant plateau line. This could be due to evaporation of volatile product(s) during drying, or polymerization. The sample decomposed due to dehydration.

Type iii: Single stage of weight loss or decomposition temperatures (Ti and Tf). the sample decomposes in one sharp step.

Type iv: Samples decompose in multi-stages, with relatively stable intermediate products.

Type v: Multi-stage decomposition with no stable intermediary. Heating rate may affect the plot, where at slow heating rate, type (5) resembles type (4) curve.

Type vi: Sample weight is increased, due to certain surface reactions (such as oxidation of metals) with atmosphere.

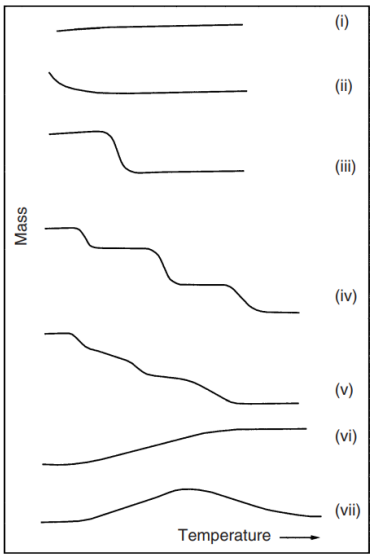

Figure 8: Classification of TGA into seven types

Type vii: Multiple reactions one after the other with respect to a rise in temperature. The increase in weight is due to the surface oxidation reaction, whereas the decrease in weight with further rise in temperature corresponds to the decomposition process, due to reduction. (Surface oxidation reaction followed by decomposition of reaction products).

3.5 Advantages (2.4):

1. It is a convenient and time-saving technique, can be easily implemented where any type of solid can be analysed with minimal sample preparation requirements.
2. It has high accuracy of balance, high precision of temperature controlling system and atmospheric conditions, allowing uniformity of the procedure.
3. Continuous recording of weight loss as a function of temperature ensures equal weightage to examination over the whole range of study.

3.6 Disadvantages (2,4):

1. TGA can study process which accompanies a mass change. Chemical or physical process which are not accompanied by the change in mass on heating or with no volatile product could not be studied. Limited to samples that undergo weight change.
2. It is very sensitive to any change, TGA is dependent on procedural details such as furnace heating rate, the atmosphere inside the furnace, sample size, or weight.
3. Interpretation of the result is not always straightforward but rather complex.
4. Operation requires high control over temperature.

3.7 Applications (2,4,13):

TGA is particularly useful for the following material characterization determinations:
1. Thermal stability: is described as the ability of a material to maintain constant characteristics when exposed to heat. TGA is used to evaluate the thermal stability of a material and is mainly used for polymers. In a desired temperature range, if a material is thermally stable, there will be no observed mass change. Negligible mass loss corresponds to little or no slope in the TGA trace.
2. Compositional analysis for samples and multi- component materials: Upon increasing the temperature of a sample, it undergoes weight loss. The weight loss profile remains significant for chemists to determine the composition of a sample so that it is possible to understand the reaction steps involved in the decomposition process and to identify an unknown compound present in the sample or examine complex materials by removing or decomposing their constituents. And also evaluate thermal decomposition mechanisms of polymers which indicates evaporation or decomposition processes of a substance.
3. Corrosion studies: TGA can be used to analyze oxidation or other reactions with different reactive gases or vapours.
4. Evaluation of moisture and volatile contents in the sample materials lost during chemical reactions, for samples such as nanomaterials, polymers, polymer nanocomposites, fibers, paints, coatings, and films.
5. TGA can estimate lifetime, shelf life of a product.
6. TGA provides quantitative measurement of mass change in materials associated with transition and thermal degradation.
7. The TGA can determine the quantity of a filler in a polymer, to estimate the additive content.

References

1. Yang Leng, 2013. Materials Characterization: Introduction to Microscopic and Spectroscopic Methods, Second Edition. Wiley-VCH Verlag GmbH & Co. KGaA. P.333- 365.

2. Kanwal Rehman and Muhammad Sajid Hamid Akash, 2020. Essentials of Pharmaceutical Analysis. Introduction to thermal analysis. ISBN 978-981-15-1547-7 (eBook). Springer Nature Singapore Pte Ltd. P 195-222. Biomat. J., 1 (12),15 – 22 (2022) 22 of 9

3. Sina Ebnesajjad, 2014. Surface and Material Characterization Techniques. Surface Treatment of Materials for Adhesive Bonding, Second Edition. Elsevier. Chapter 4, P. 62-70.

4. Euth Ortiz Ortega, Hamed Hosseinian, Ingrid Berenice Aguilar Meza, Maria Jose Rosales Lopez, Andrea Rodriguez VerA, 2022. Characterization Techniques and Applications. Chapter 5: Characterization Techniques for Thermal Analysis. Springer. P. 153- 180.

5. Haines, P. J., Reading, M., & Wilburn, F. W. (1998). Differential Thermal Analysis and Differential Scanning Calorimetry. Handbook of Thermal Analysis and Calorimetry, 279–361.

6. https://resources.perkinelmer.com/labsolutions/resources/docs/TCH_Guide-to-DSC-Selection-Pans.pdf accessed on November 24th, 2022.

7. https://resources.perkinelmer.com/lab-solutions/resources/docs/tch_guideto-dsc-selection-pans.pdf.

8. https://en.wikipedia.org/wiki/Differential_scanning_calorimetry accessed on November 23rd, 2022.

9. El-Zeiny Ebeid, Mohamed Hegazy, 2021. Thermal Analysis: From Introductory Fundamentals to Advanced Applications, First Edition. Elsevier science.

10. Demetzos, C., & Pippa, N. (Eds.). (2019). Thermodynamics and Biophysics of Biomedical Nanosystems. Series in BioEngineering.

11. https://polymerscience.physik.hu-berlin.de/docs/manuals/DSC.pdf accessed on November 25th ,2022.

12. https://resources.perkinelmer.com/labsolutions/resources/docs/faq_beginners-guide-to-thermogravimetric-analysis_009380c_01.pdf accessed on November 25th ,2022.

13. Loganathan, S., Valapa, R. B., Mishra, R. K., Pugazhenthi, G., & Thomas, S. (2017). Thermogravimetric Analysis for Characterization of Nanomaterials. Thermal and Rheological Measurement Techniques for Nanomaterials Characterization. P. 67–108.

Biomaterials Journal
http://www.biomatj.com
Online ISSN: 2812-5045

Type of the Paper (Research Article)

Lipid polymer hybrid nanoparticles as targeted drug delivery system for melanoma treatment

Arooj Naeem[1]*, Samia A. Khan[2], Hamza A. Khan[3]

[1] *First Affiliation, student of university of Gujrat, 19011560-010@uog.edu.pk, Jhelum and 49600, Pakistan*

[2] *Second Affiliation, student of pharmacy,Lahore and 54728, Pakistan*

[3] *Third Affiliation, lecturer at Islamic university, Islamabad and 04405, Pakistan*

* Corresponding author e-mail:

Citation: ***Arooj Naeem, Samia A. Khan, and Hamza A. Khan . Lipid polymer hybrid nanoparticles as targeted drug delivery system for melanoma treatment*** *. Biomat. J., 2 (1),24 – 39 (2023).*

https://doi.org/10.5281/znodo.5829408

Received: 23 January 2023
Accepted: 30 January 2023
Published: 31 January 2023

Abstract: Our understanding of the biologic effects (including toxicity) of nanomaterials are incomplete. In vivo animal studies remain the gold standard; however, widespread testing remains impractical, and the development of in vitro assays that correlate with in vivo activity has proven challenging. Here, we demonstrate the feasibility of analysing in vitro nanomaterial activity in a generalizable, systematic fashion. We assessed nanoparticle effects in a multidimensional manner, using multiple cell types and multiple assays that reflect different aspects of cellular physiology. Hierarchical clustering of these data identifies nanomaterials with similar patterns of biologic activity across a broad sampling of cellular contexts, as opposed to extrapolating from results of a single in vitro assay. We show that this approach yields robust and detailed structure–activity relationships. Furthermore, a subset of nanoparticles was tested in mice, and nanoparticles with similar activity profiles in vitro exert similar effects on monocyte number in vivo. This data suggests a strategy of multidimensional characterization of nanomaterials in vitro that can inform the design of novel nanomaterials and guide studies of in vivo activity.

Keywords: *Lipid polymer hybrid nanoparticles; melanoma cancer; nanocarriers; vitamin D receptors; bioactivity; targeted drug delivery system.*

I. Introduction

Melanoma occur as a result of genetic alterations in the cell which produce the pigment known as melanocytes[1]. Although melanoma accounts only 4 percent but it is responsible for highest number of deaths related to skin cancer[2]. Till date, the most commonly utilized treatment for melanoma cancer is chemotherapy, but it may also contain very serious side-effects on healthy cells of body, lesser bio-availability, poor selectivity on the way to tumor[3]. Another problem is that when chemotherapeutic drugs are utilized for the extended period of time, it results in developing MDR (multidrug resistance)[4]. If the treatment target just tumor cells, then side effects would be minimized. In case of melanoma, it shows very less response rate towards the conventional form of therapies that are present[5]. Nanocarries have been extensively utilized for delivering drug to targeted site of action which results in higher therapeutic efficiency[6]. The size of nanoparticles (NPs) ranges from the one to thousand nm (nanometers) in diameter. The diverse physio-chemical proper-

ties of nanoparticles e.g. size and of NPs, surface-area and surface charge of NPs give them benefit over current anti-cancerous treatments[7].

The most commonly utilized nanocarriers comprise of polymeric drug delivery system (DDS) and vesicular system based on the lipid[8]. Polymeric NPs show tremendous medicine loading and stability but less bio-compatibility, but in comparison, liposomes display very good biocompatibility but they face the complications of leakage of drug[9]. In order to overcome the limitations of NPs and liposomes, a new class of drug delivery system known as LPNPs (lipid polymer hybrid nanoparticles) has been established which contain properties of both liposomes and polymeric molecules which comprises of 3 parts, a bio-degradable polymeric core which is hydrophobic in nature and contain hydrophobic drug, and in order to enhance the system biocompatibility a single layer of phosphor-lipids which surround the core is present and then in order to rise the systemic circulation life-time and the stability, a hydrophilic polymer layer present outside the lipid[10]. In order to develop the lipid polymer hybrid nanoparticles, countless polymers have been designed which include PLGA (poly lactic co glycolic acid), PLA (polylactic acid), PbA (poly β amino ester and chitosan, these polymers are extremely bio-degradable and have high compatibility[11]. Like numerous varieties of nanocarrier, polymer lipid nanoparticles can also couple with targeting moieties so that the drug delivers precisely to the cells of tumour and tumour vasculature[12].

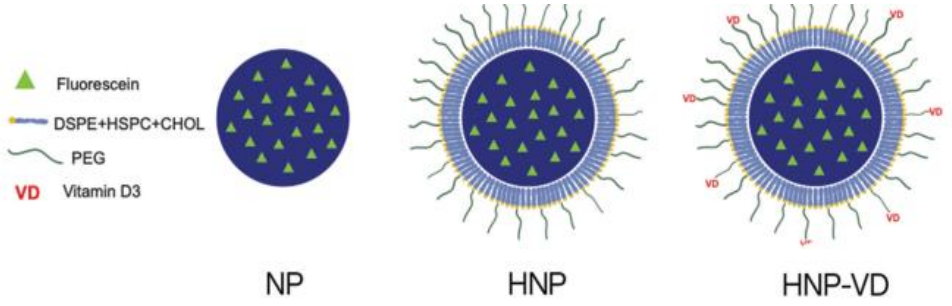

Figure 1. PLGA NP (nanoparticles), HNP (hybrid lipid polymer nanoparticles), HNP-VD (vitamin D3 functionalized hybrid lipid polymer nanoparticles)

These hybrid lipid polymer NPs have several benefits e.g., circulate for extensive period of time, higher capacity of drug loading, higher stability and property of controlled release[13]. PLGA (poly lactic co glycolic acid) nanoparticles are widely utilized for the delivery of therapeutic drugs due to their capability of maintain the drug for extended period of time, their compatibility[14]. These hybrid particles comprise of the poly lactic co glycolic acid (PLGA) as core and 2 lipids DSPE-PEG and HSPC (hydrogenated-soy phosphatidylcholine) form the shell which basically surround the particle and among lipids, the molecule of cholesterol play very important part in stabilizing the membrane[15]. HNPs (hybrid NP) were manufactured with folic acid in order to specifically delivering the paclitaxel against the cervical cancerous cells[16]. In order to enhance efficacy of hybrid nanoparticles, it was first time these hybrid NPs are basically coupled with ligand such as vitamin D which comprise of 2 main forms (Vitamin D2 and vitamin D3)[17]. Studies have indicated that vitamin D receptor (VDR) is present in body including skin and it is also located in melanoma cell[18]. The activated form of VD is the vitamin D3 (1,25 di-hydroxy

vitamin D3) which employs its effect on targeted tissue by activating the VDR[19]. This was first time in which HNP-VD (lipid polymer hybrid NPs with functionalized VD3) was synthesized in order to target the receptors of vitamin D and enhance the cell internalization and in this VD3 covalently attached to DSPE-PEG2000[20].

2. Material and Methods

Poly lactic co glycolic acid (PLGA 50:50) was donated by PURAC (Germany). The solvents EtAc (ethyl acetate), dichloro-methane (DCM) and dimethyl-sulfoxide (DMSO) were bought from Merck (Germany). Poly vinyl -alcohol (PVA), fluorescein, trehalose, cholesterol (CHOL), iron-III-chloride hexahydrate and ammonium thiocyanate were attained from Sigma-Aldrich (Germany). Chloroform was attained from Fisher Scientific in USA. For the synthesis of the HNPs, hydrogenated soy phosphatidyl-choline (HSPC), 1,2-disteroyl-sn-glycero-3-phosphaethanolamine-N-[succinyl(polyethylene glycol)-2000 (DSPE-PEG2000) and 1,2-distearoyl-sn-glycero-3-phosphoethanolamine-N-[cholecalciferol(polyethylene glycol)-2000] (DSPE-PEG2000-VD) were bought from Nano soft Polymers. In addition, all reagents for cell culture were bought from Gibco/Invitrogen (Life Technologies - Carlsbad, CA, United States).

2.1. Synthesis of PLGA nanoparticles

The manufacturing of polymeric nanoparticles, lipid-polymer hybrid nanoparticles and functionalized lipid polymer hybrid nanoparticles (Figure 1) were carried out according to the following procedures [21]. The manufacturing of the PLGA NPs was carried out by means of the solvent evaporation emulsification method. For individual sample, 50 mg of PLGA were evaluated and dissolved in 1 mL of a EtAc: DMSO (3:1) solution. Samples containing fluorescein and Nile-red were prepared by thawing 1.25 mg and 0.5 mg in the solvent phase, respectively. 2 aqueous solutions of PVA (0.3 and 3.0% w/v) were set and 25 mL of the 0.3% (w/v) solution was shifted into a 50 mL beaker and agitated at 250 rpm. 2 mL of the 3.0% (w/v) solution was further added to a 15 mL centrifuge tube. Subsequently, the PLGA solution was added dropwise to the centrifuge tube under forceful vortexing. Once the whole volume was added, 30 seconds of extra vortexing was conducted. Afterward, the centrifuge tube was placed on an ice bath and transferred to a probe ultra-sonicator for 30 seconds (60% amplitude and 8 W). This process (vortex 30 s/ultra sonicator 30 s) was repeated 3 times. Finally, the dispersion was moved to the 0.3% (w/v) PVA solution where the nanoparticles were permitted to harden for 12 h. NPs collection was led by transferring the dispersion to an Oak Ridge tube and centrifuging at 25,000 rcf for 60 minutes. After, the supernatant was wasted, and the particles were re-suspended in deionized water. This washing step was repeated 3 times. The NPs were then re-suspended in a trehalose: polymer (1:2) solution, frozen in liquid N2 and lyophilized for 72 hours.

2.2. Synthesis of hybrid lipid-polymer nanoparticles (HNPs)

HNPs were manufactured using the gentle hydration method. This method contains of the formation of a lipid thin film in a round bottom flask followed by the hydration of this layer by a dispersion of NPs. In this work, the hybrid NPs were

formed with and deprived of the presence of targeting ligands. Briefly, a mixture of lipids HSPC: CHOL:DSPE-PEG-2000 (2:1:0.1 molar ratio) was dissolved in 5 mL of CHCl3. Then, the solvent was evaporated by means of a rotary evaporator, producing a thin lipid-film on the wall of the round bottom flask. The NPs formerly prepared were re-suspended in 5 mL of deionized water (6 mg/mL), added to the round bottom flask containing the lipid film at 1 mL/min and sonicated for 10 min. The round bottom flask was transferred to a stirring plate and the HNPs were leftward to self-assemble for 30 min under mild stirring and then lyophilized. The HNPs containing the targeting ligand (HNP-VD) were set using the same method, however, the combination of lipids was substituted by HSPC: CHOL: DSPE PEG2000: DSPE PEG2000-VD (2:1:0.08:0.02 molar ratio). Furthermore, aiming to enhance the amount of lipids utilized in the synthesis, HNPs were ready by means of the following lipid: NPs ratios: 1:1, 1:10, 1:20 and 1:25 (w/w). Table 1 show amount used for various samples.

Table 1. Equivalents utilized in formation of HNPs for various lipid: NPs ratio.

Mass ratio (Lipid:NPs)	Molar ratio	M_w (g/mol)	mg	mmol
1:1				
HSPC	2	785	20.8	0.02650
CHOL	1	387	5.1	0.01320
DSPE-PEG_{2000}	0.1	2993	4.1	0.00140
1:10				
HSPC	2	785	1.92	0.00240
CHOL	1	387	0.52	0.00130
DSPE-PEG_{2000}	0.1	2993	0.40	0.00010
1:20				
HSPC	2	785	1.06	0.00130
CHOL	1	387	0.27	0.00070
DSPE-PEG_{2000}	0.1	2993	0.20	0.00007
1:25				
HSPC	2	785	0.70	0.00090
CHOL	1	387	0.20	0.00040
DSPE-PEG_{2000}	0.1	2993	0.10	0.00004

2.3. Characterization of the nanoparticles

The NPs and HNPs were categorised by FEG-SEM (field emission scanning electron microscopy), DLS (dynamic light scattering) and zeta potential. Microscopy investigations were achieved on the equipment FeiVR Inspect F-50. The images were gotten applying a drop of an aqueous solution of NPs or HNPs (100 mg/mL) directly to the top of the stub. Next, the samples were exposed to gold sputtering for 80s. The parameters for the imagining of particles were distance of 7–8 millimetre's, 20 kilovolt and magnification of 70,000–300,000. The determination of the hydrodynamic diameter, achieved by DLS, along with the zeta potential analysis, were conducted on the ZetaSizer Nano series equipment from Malvern, England.

2.4. Quantification of lipid surface coverage

The process of quantification of lipids on the surface of HNPs, defined, is based on 2 analyses.1st, a colorimetric assay was utilized in which the creation of complexes of phosphor-lipids with ammonium ferro-thiocyanate are quantified. Another, a H-NMR analysis is made to enumerate the amount of DSPE-PEG2000 present on the surface of the HNPs from the proton absorptions of lactate units (5.19 parts per million), glycolate units (4.91 parts per million) and ethylene oxide units (3.51 parts per million). The primary method was applied by thawing 2 mg of HNPs formed with dissimilar polymer/lipid ratios (1:1, 1:10, 1:20, 1:25 w/w) in CHCl3. The resultant solution was diverse with 2 mL of the ammonium ferro-thiocyanate solution and then vortexed (60 s) to form the complex. The subsequent mixture was centrifuged at small speed and the absorbance of HSPC/AF complexes were measured at the wavelength of 471 nm. The amount of lipids was considered by means of a standard curve beforehand set with the similar lipid composition of the shell of the HNPs. The typical solution of ammonium ferro-thiocyanate was set according to Stewart [29]. Momentarily, 27.03 g of iron-III-chloride hexahydrate and 30.4 g of ammonium thiocyanate were dissolved in 1 L of deionized water. Then, a 2:1:1 (molar ratio) combination of HSPC, CHOL and DSPE-PEG2000 was thawed in 100 mL CHCl3. Volumes between 0.1 and 1.0 mL of this solution were further added to 2 mL of the ammonium ferro-thiocyanate solution in a centrifuge tube and sufficient CHCl3 was further added to bring the ending volume to 4 ml. The system was vortexed for 1-minute, the organic-phase detached using a Pasteur pipette and at that moment added to a cuvette for absorbance study through UV/ Vis (wavelength 471 nm). From the values attained, the quantity of lipids per milligram of HNPs, the number of lipids per HNPs and the % of coating of HNPs can be calculated by Eqs.1–3, respectively.

$$V_1 = \frac{M_L / Mw_L}{M_{NPs}} \quad (1)$$

$$V_2 = V_1 N_A V_{NPs} \rho_{PLGA} \quad (2)$$

$$V_3 = \frac{V_2 S_L \times 100\%}{S_i} \quad (3)$$

Where V1 is the quantity of moles of lipids per mg of HNP, V2 is the amount of lipids per HNP and V3 is the % of coating of the HNP. ML is the mass of lipids utilized in the preparing the HNP, MNPs is the mass of nanoparticles examined, MwL is the molecular weight of lipids, VNPs is the individual volume of individually NP, ρPLGA is the density of PLGA and NA is the Avogadro-number. Si is the surface area of a single NP and SL is the area of the polar portion of the HSPC and DSPE-PEG2000 molecules, are assumed by 0.694 nm2 and 1.240 nm2, correspondingly.

2.5. Drug release study

In this work, the release of the perfect drug fluorescein from NPs, HNPs and HNP-VDs were achieved in triplicate by means of the dialysis method for 6 days. For individual experiment, 5 mg of sample were distributed in 1 mL of the release medium (PBS, pH 7.4, 0.01 M) and positioned in contact with the dialysis membranes (Mw cut-off =14,000 Dalton) in the Franz cell donor section (Automated Franz Cells –

Microette Plus, Hanson Research Corporation, USA). The receiver section, where 7 mL of the release medium were located, was sustained under constant moving at a temperature of 320C. At predetermined intermissions (0.5, 1, 2, 4, 8, 12, 24, 48, 72, 96, 120 and 144 h), 1 mL aliquot was with-drawn from the recipient medium and the same volume of PBS further added to preserve the infinite dilution condition. Examination of samples taken at diverse times were performed by spectrofluorimetric in a plate reader (Molecular Devices – SpectraMax M2e). To attain the encapsulation efficiency (EE) and drug loading efficiency, the methodology presented was utilized and their values can be considered according to Eqs. 4 and 5. Momentarily, 2 mg of fluorescein loaded nanoparticles were dissolved in 1 mL of aceto-nitrile and then added to 10 mL of PBS in order to disperse the PLGA from the fluorescein. Then, the PLGA was sieved through a cellulose filter (pore size: 0.2 mm) and the solution examined by UV/Vis at a fixed wavelength 490 nm. The concentration of fluorescein present in the examined nanoparticles was then considered from a calibration curve.

$$EE = \frac{\text{weight of drug in NPs} \times 100\%}{\text{weight of drug added}} \quad (4)$$

$$DL = \frac{\text{weight of drug in NPs} \times 100\%}{\text{weight of NPs}} \quad (5)$$

2.6. Cell culture

B16 cell line, illustrative of mouse melanoma, was bought from the American Cell Culture Collection (ATCC). Cells were grown-up in Dulbecco's Modified Eagle Medium added with 10% fetal bovine serum (FBS), penicillin/ streptomycin (100 U/mL) and fungizone. Furthermore, the cells were maintained at the temperature of 370C, 95 percent air humidity and 5 percent CO2.

2.7. In vitro cell viability assay

The assessment of cell viability was performed as described by means of B16 melanoma cells. Momentarily, 6.5103 cells were seeded in 96 well-plates and upheld under optimum culture conditions till reaching 70% convergence. After this period, the cells were treated with dissimilar concentrations of nanoparticles (10, 50, 100 and 500 μg/mL) formerly filtered (0.45 μm filter) in their different NP, HNP and HNP-VD formulations. Cells were upheld 24 h after treatment and later they were submitted to cell viability examination. Firstly, cells were wash away with PBS and incubated with a solution of 3-(4,5-dimethylthiazol-2- yl)-2,5-diphenyltetrazolium bromide (MTT) (Sigma Aldrich, Inc.) (5 mg/mL) diluted in DMEM 10% of FBS. The crystals of formazam, a product of the mitochondrial redox reaction of viable cells, were dissolved in 100 μL of dimethyl-sulfoxide (DMSO), and the staining intensity was determined by the Spectra-Max M2e-Molecular Devices equipment at wavelength 570 nm. The absorbance was directly proportional to the amount of living cells with active mitochondria. The results were expressed as % in relation to the control without treatment.

2.8. Cellular uptake

To assess the cellular uptake of the nanoparticles, B16 melanoma cells were treated with the dissimilar formulations containing the fluorescent marker Nile-red. Cells (2.010^4) were seeded in 24 well-plates and incubated under perfect conditions of cultivation for 24 hours. After, cells were treated for 3 hours with NP, HNP and HNP-VD, containing NR, at the concentrations of 50 and 100 μg/ml. Then, the culture medium was detached, the cells were washed 3 times with PBS and analysed through inverted fluorescence microscopy (Olympus IX71VR).

2.9. Statistical analysis

For the evaluation of the results, the ANOVA one-way test was used, followed by Tukey post-hoc test. The results were expressed as mean ± standard error. The GraphPad Prism 5.0VR program was used to evaluate the results and to generate the graphs. $p < 0.05$ was considered significant.

3. Results and discussion

3.1. Synthesis of NP, HNP and HNP-VD

PLGA nanoparticles (NPs) were manufactured by the simple emulsification or solvent evaporation method. This practise is extensively reported in the literature for the making of polymeric NPs for various applications. The NPs were formed with properties such as size, zeta potential and PDI (polydispersity index) appropriate for application in drug delivery systems (Table 2). Among these properties, the small PDI was detected, confirming the homogeneousness of the sample magnitude distribution. From the images obtained in the FEG-SEM (Figure 2) it is probable to confirm the round morphology of the NPs as well as to check the size and the narrow distribution data detected via DLS.

As expected, rise in the size of the NPs occurred after addition a lipid layer on its surface. The PDI also amplified significantly. This may be due to the excess number of phospholipids resulting in the creation of micelles with dissimilar sizes and without a polymeric core in the stage of combination of these particles. Therefore, the use of 1:1 mass ratio (lipids: NPs) may lead to a difficulty in the manufacturing step due to the possible concurrent formation of lipid micelles. The zeta potential did not display any important rise in its value after the introduction of the lipid layer. The negative charges are a result of the presence of terminal carboxyl groups in the polymer. According to [22], the lipid-to-polymer ratio used in the combination of HNPs should be optimized since, when in surplus, lipids may synthesize micelles and liposomes absent of the polymeric core, which is reliable with our results. This fact can lead to accumulation and loss of active ingredients during the purification procedure.

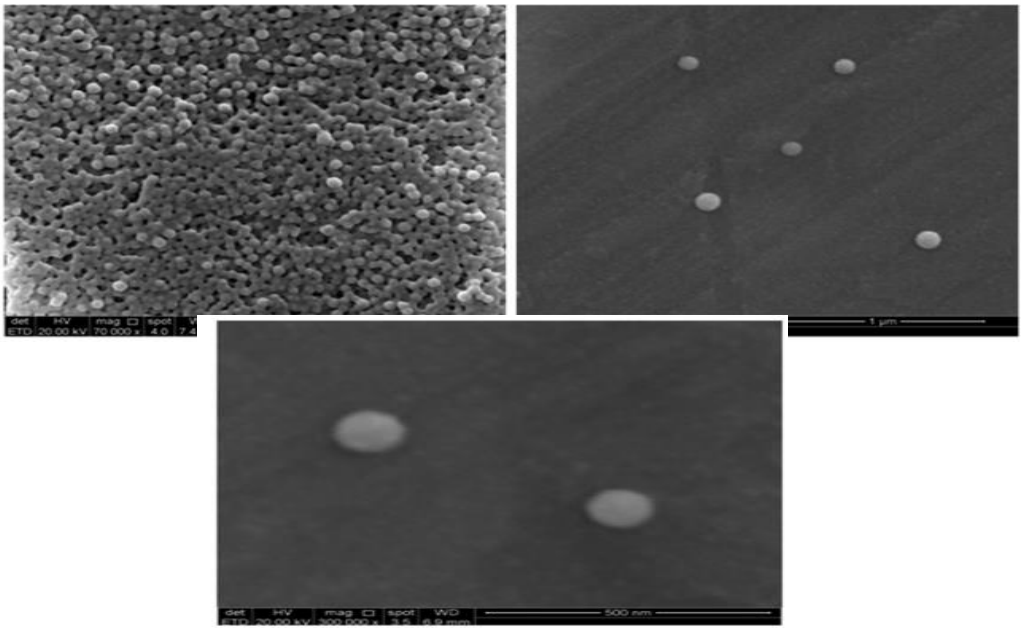

Figure 2. FEG SEM images from synthesized nanoparticles at 70,000x, 120,000x and 300,000x

Table 2. Characterization of NPs and HNPs by utilizing 1:1 lipid: NPs mass ratio.

Sample	Diameter (nm)	PdI	Zeta potential (mV)
NPs	133.6 ± 0.3	0.058 ± 0.012	−14.30 ± 0.70
NPHs	256.8 ± 38.4	0.286 ± 0.100	−13.59 ± 3.15

3.2. Optimization of lipid-to-polymer ratio

To evade the development of micelles without polymeric core and the extreme use of lipids to cover the HNPs, the coverage % of the lipid layer on the NPs was enumerated and the mass ratio (lipid: NPs) utilized in the synthesis was optimized using the following mass ratios: 1:10, 1:20 and 1:25 (w/w).

The HNPs were categorised as described formerly for the NPs and the results obtained are summarized in Table 3. As the ratio of lipid: NP declines, the particle size decreases, demonstrating that the lipid layer is less dense when less lipid is used to form the HNPs. The PDI was lower for particles formed with less lipid (1:10, 1:20 and 1:25) than those shaped with the highest ratio (1:1). The lower PDI shows that fewer, if any, lipid micelles may be forming. No noteworthy change in zeta potential was detected when reducing the lipids: NPs mass ratio.

Table 3. Characterization of HNPs formed with varying lipid: NPs mass ratio.

Lipid:NPs	Diameter (nm)	PdI	Zeta potential(mV)
1:1	256.77 ± 38.40	0.286 ± 0.10	−13.59 ± 3.15
1:10	209.80 ± 0.001	0.190 ± 0.19	−15.0 ± 1.56
1:20	189.30 ± 2.69	0.222 ± 0.08	−11.4 ± 2.19
1:25	163.20 ± 8.23	0.183 ± 0.01	−14.0 ± 1.30

The HNP coating % calculations can be achieved from the colorimetric method presented by Stewart together with H-NMR analysis, as presented [23]. The results of the H-NMR analysis are accessible in Figure 3, where the spectra provide the value of the proton integration of lactate, glycolate and ethylene oxide units. By calculating the ratio between these peaks, it is likely to quantify the % of DSPE-PEG2000 in the sample. Analysing the results, the ratios attained were 1.93:1, 6.92:1, 10.9:1 and 12.7:1 for the mass ratios of 1: 1, 1:10, 1: 20 and 1:25, correspondingly. The values attained for each compound relative to surface lipid density, molecules per NP and coating % are shown in Table 4. The total coverage % is given by the sum of the partial coverages of HSPC and DSPE-PEG2000. The total value for each mass ratios used in the HNPs preparations is shown in Figure 4.

As exposed in Figure 4, the mass ratio of 1:25 displays a NP coating of 97% and, therefore, it was determined that this ratio is optimal for the manufacture of HNPs and HNP-VDs. This condition is like to the work presented by Desai, where the authors used a 1:15 ratio, and where a ratio ranging from 10 to 20% was measured optimal. It is important to note that, in their work, the nano-precipitation method for the synthesis of the hybrid NPs was utilized but the polymer was not PLGA. Those who achieved the HNP preparation in two stages utilized the ratio of 1:1, but do not state the % of area covered by the phospholipid layer.

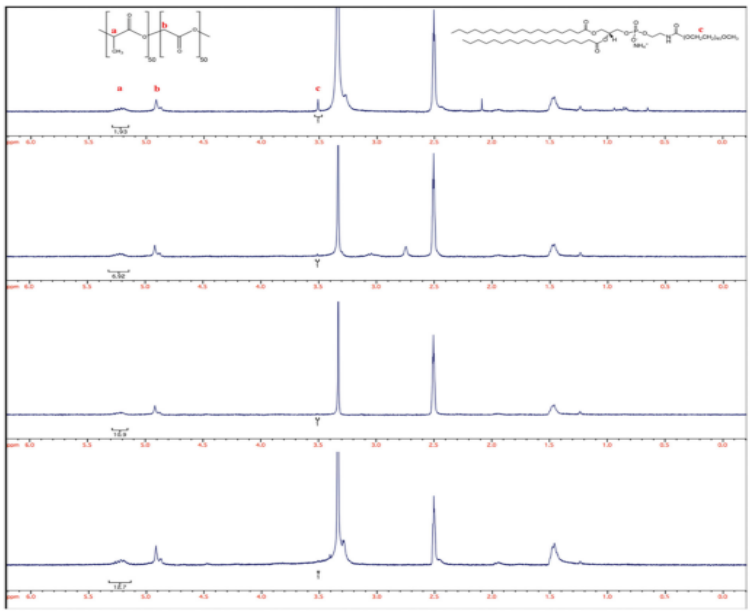

Figure 3. H-NMR spectra of hybrid nanoparticles synthesized. from top to bottom lipid; NPs mass ratio of 1:1, 1:10, 1:20 and 1:25.

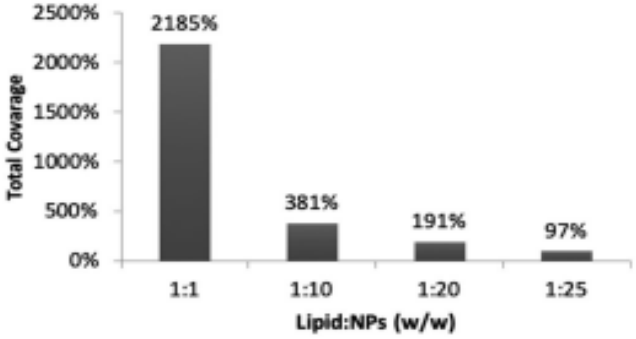

Figure 4. Total coverage of nanoparticles by utilizing various lipids: NPs ratios.

Table 4. Lipid quantification on surface of HNPs.

	HSPC			$DSPE\text{-}PEG_{2000}$		
Lipid:NPs (w/w)	Surface density (nmol mg^{-1} NP)	Molecules per NP (10^4)	Coverage (%)	Surface density (nmol mg^{-1} NP)	Molecules per NP (10^4)	Coverage (%)
1:1	544.8 ± 15.0	554.1 ± 15.2	1394 ± 38	172.9	175.8	791
1:10	106.1 ± 3.1	50.2 ± 1.4	210 ± 6	48.3	22.9	171
1:20	62.7 ± 3.5	16.4 ± 0.9	102 ± 6	30.6	8.0	89
1:25	24.4 ± 1.6	3.8 ± 0.3	33 ± 2	26.2	4.1	64

All of the HNPs and HNP-VDs used then in this work for drug release studies, In vitro cell viability and cellular uptake valuation were produced according to the improved fabrication conditions (1:25 lipid: NPs mass ratio). The results obtained from the description of the nano-carriers manufactured with the optimal conditions are described in Table 5. As expected, the diameter of the NPs rises when the phospholipid layer is introduced. Likewise, the HNPs that contain the vitamin D3 ligand (HNP-VDs) are to some extent larger than those without the ligand. However, zeta potential is unpretentious by the addition of the ligand. Figure 5 shows the images obtained by FEG-SEM of the samples HNP and HNP-VD.

Table 5. NPs, HNPs and HNP-VDs formed with optimal conditions.

	Diameter (nm)	PDI	Zeta potential (mV)
NPs	133.6 ± 0.3	0.058 ± 0.012	−14.3 ± 0.7
NPHs	163.2 ± 6.7	0.184 ± 0.011	−14.0 ± 1.1
NPHs-F	175.4 ± 6.5	0.199 ± 0.011	−13.9 ± 0.1

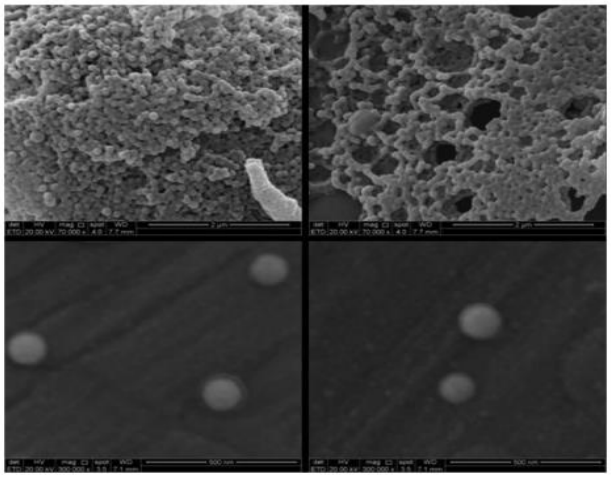

Figure 5. FEG SEM images from hybrid nanoparticles (left) and hybrid nanoparticles-vitamin D3 (right) synthesized with optimized lipid: NP ratio (1:25)

3.3. Drug release study

To perform release kinetics studies, NPs, HNPs and HNP-VDs comprising fluorescein were fabricated and the release studies were conducted over 6 days. The amount of fluorophore encapsulated within individual nanocarrier was enumerated and the results are shown in Table 6. In the first 24 h of incubation, 75, 62, and 57% of the fluorescein in the NPs, HNP, and HNP-VD were released correspondingly, configuring a burst release. For the consequent period, a slower release was detected where the cumulative release of fluorescein from the NPs was 88%, 75% for the HNP and 68% for the HNP-VD (Figure 6). The release behaviour is alike to the work presented where the total % released from the NPs was the uppermost followed by HNP and HNP-VD. It is hypothesized that this occurs because introducing the lipid layer rises the diffusion distance of the fluorescein, as does adding the targeting ligand (according to nanoparticle diameters in Table 6). The lipid layer may also affect division of the fluorescein within the nanoparticle, further hindering its release.

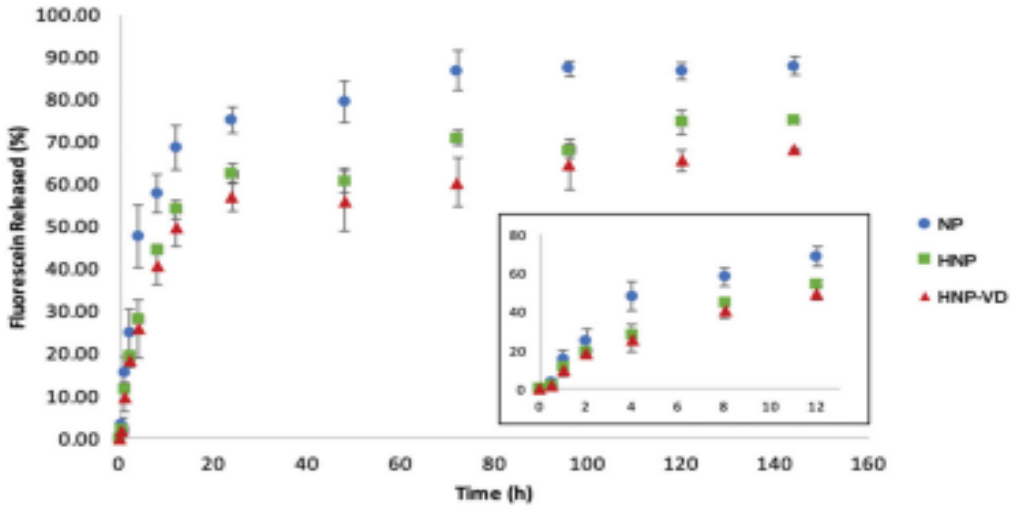

Figure 6. Fluorescein release behavior in PBS at pH 7.4; 0.01 M; 320C for the various samples.

3.4. In vitro cell viability

To validate the effect of the nanoparticles on cell viability, the diverse formulations (NP, HNP, and HNP-VD) were incubated with the B16 melanoma line [24], and the MTT assay was accomplished after 24 hours. After this period, the viability protocol was accomplished as described in the methodology, and results were expressed as a % relative to the untreated control. As depicted in Figure 7, cell viability was not changed with all the formulations tested, although it was detected a reduction of viable cells at the highest nanoparticle concentration (500 μg/mL) for HNP and HNP-VD, but the results were not statistically noteworthy. Notably, cells incubated with the HNP-VD formulation at 50 mg/mL exhibited a noteworthy rise in viability after 24 hours, demonstrating cell proliferation. Preceding study has shown that the activation of VD-VDR can encourage a proliferation stimulus to melanoma cells. The results attained here showed HNP-VD formulation as an important drug delivery system in melanoma cells.

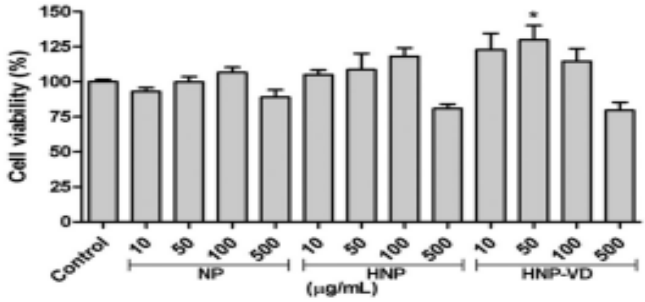

Figure 7. Evaluation of the cellular sustainability of B16 cells after treating with NP, HNP and HNP-VD preparations at conc. of 10, 50, 100 and 500 μg/ml.

Cells were upheld under optimal culture conditions for 24 hours under treatment. After this period, the viability protocol was achieved as described in the methodology. The results are expressed as a % relative to the untreated control. The experiments were performed 3 times in triplicate.

3.5. Cellular uptake study

Nanoparticle uptake by melanoma cells was assessed using fluorescence microscopy. After 3 hours of incubation with various formulations, it was detected that there was a alteration in the cellular distribution of the nanoparticles according to their specific formulation (Figure 8). NP (A) and HNP (B) HNP-VD (C) had more important localization in the cytoplasmatic and perinuclear domains, as indicated in Figure 8. After the incubation with the various nanoparticle preparations (NP, HNP and HNP-VD) at concentrations of 10 and 100 μg/mL, the cells were kept under optimal culture conditions for 3 hours and the fluorescence amount was assessed by an

inverted microscope. The images were taken from an objective with a 40x magnification. To facilitate the image of the proximity of HNP-VD to the nucleus of B16 melanoma cells, Figure 9 indicates the images obtained by brightfield and fluorescence microscopy, and the merged image utilizing a higher magnification power (400x). The images taken here clearly demonstrated that the HNP-VD nanoparticles were localized close to the nucleus of melanoma cells. This suggests that HNP-VD nanoparticles may be well-suited to provide therapeutics to the cell nucleus. Other studies have indicated the benefit of the internalization of NPs by tumour cells. It showed that the uptake of Nile-Red labelled NP by breast were placed nearer to the membrane of cells with decreased cytoplasmic distribution. On the other hand, cancer MCF-7 cells better the intracellular delivery of the encapsulated drug.

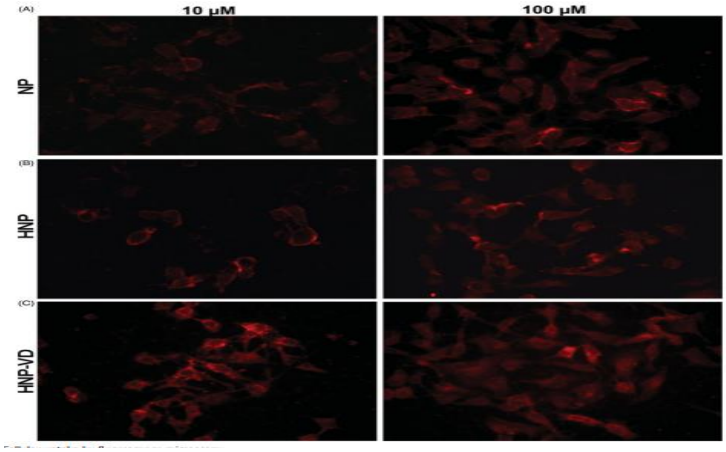

Figure 8. Cellular uptake by FM (fluorescence microscopy).

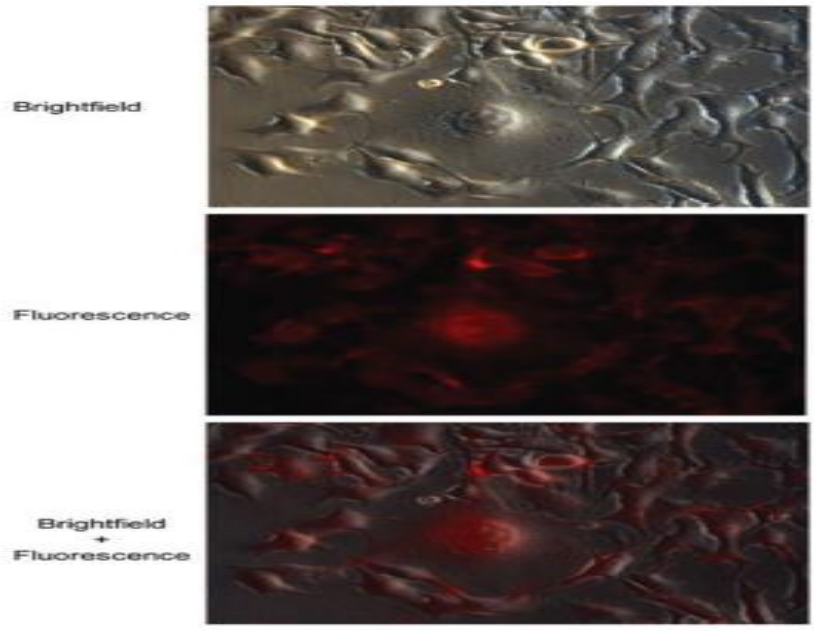

Figure 9. Cellular uptake and localization of HNP-VDs at the conc. of 100 µg/ml. The images were taken from an objective with magnification power of 400x.

4. Conclusion

This work presents the production of lipid nanoparticle hybrids, with (HNP-VDs) and without (HNPs) a pointing receptor in the surface. The mass ratio of lipid: NP was improved to obtain the optimum amount of lipids on the surface of the nanoparticles. According to the colorimetric process and the H-NMR study, HNPs were produced with 97 percent of their surface area covered by the lipid layer. In vitro release of fluorescein demonstrated an initial burst release of 75, 62, and 57 percent during the first 24 hours for NPs, HNP, and HNP-VD, respectively, followed by a gentler release for the left time. These results suggest that the nano-carriers used in this work can be used as regulated drug delivery systems for substances containing physio-chemical properties like fluorescein. Moreover, we can assume that the NPs and HNP did not promote considerable effects on melanoma B16 cells, though, HNP-VD lead to an increase of cell proliferation, probably due the communication VD-VDR. Cellular uptake data suggested that HNP-VD was concentrated in the perinuclear region of B16 melanoma cells, apparently due to the presence of the ligand vitamin D which affects nuclear receptor VDR. These results prove that HNP-VD is a good candidate for the development of affected melanoma treatment protocols as well as the specific transfer of encapsulated therapeutic agents to other cells containing nuclear VDR (vitamin D receptors).

5. Acknowledgement

The authors are grateful to the National Council for Scientific and Technological Development (CNPq) and Coordination for the Improvement of Higher Education Personnel (CAPES) for the Science without Borders Scholarship.

6. Conflict of interest

There is no conflict to declare.

References

1. Domingues, B., et al., *Melanoma treatment in review.* ImmunoTargets and therapy, 2018. **7**: p. 35.

2. Mishra, H., et al., *Melanoma treatment: from conventional to nanotechnology.* Journal of Cancer Research and Clinical Oncology, 2018. **144**(12): p. 2283-2302.

3. Wang, H. and W. Sheng, *131I-Traced PLGA-Lipid Nanoparticles as Drug Delivery Carriers for the Targeted Chemotherapeutic Treatment of Melanoma.* Wang and Sheng Nanoscale Research Letters, 2017. **12**: p. 365.

4. Rizwanullah, M., et al., *Polymer-Lipid Hybrid Nanoparticles: A Next-Generation Nanocarrier for Targeted Treatment of Solid Tumors.* Current Pharmaceutical Design, 2020. **26**: p. 1-11.

5. Arasi, M.B., et al., *Advances in Natural or Synthetic Nanoparticles for Metastatic Melanoma Therapy and Diagnosis.* Cancers, 2020. **12**(10): p. 2893.

6. Scopel, R., et al., *Lipid-polymer hybrid nanoparticles as a targeted drug delivery system formelanoma treatment.* INTERNATIONAL JOURNAL OF POLYMERIC MATERIALS AND POLYMERIC BIOMATERIALS, 2022. **71**(2): p. 127-138.

7. Mohanty, A., S. Uthaman, and I.K. Park, *Utilization of Polymer-Lipid Hybrid Nanoparticles for Targeted Anti-Cancer Therapy.* Molecules 2020. **25**: p. 4377.

8. Bhattacharya, S., *Methotrexate-loaded polymeric lipid hybrid nanoparticles (PLHNPs): a reliable drug delivery system for the treatment of glioblastoma.* Journal of Experimental Nanoscience, 2021. **16**(1): p. 344-367.

9. Song, M., et al., *Nanocarrier-based drug delivery for melanoma therapeutics.* International Journal of Molecular Sciences, 2021. **22**(4): p. 1873.

10. Wu, B., et al., *Folate-containing reduction-sensitive lipid–polymer hybrid nanoparticles for targeted delivery of doxorubicin.* Biomaterials science, 2015. **3**(4): p. 655-664.

11. Persano, F., G. Gigli, and S. Leporatti, *Lipid-polymer hybrid nanoparticles in cancer therapy: Current overview and future directions.* Nano Express, 2021. **2**(1): p. 012006.

12. Wu, X.Y., *Strategies for optimizing polymer-lipid hybrid nanoparticle-mediated drug delivery.* 2016. **13**(5): p. 609-612.

13. Tan, S., et al., *Lipid-enveloped hybrid nanoparticles for drug delivery.* 2013. **5**: p. 860.

14. Acharya, S. and S.K. Sahoo, *PLGA nanoparticles containing various anticancer agents and tumour delivery by EPR effect.* Advanced drug delivery reviews, 2011. **63**(3): p. 170-183.

15. Hu, Y., et al., *Engineering the lipid layer of lipid-PLGA hybrid nanoparticles for enhanced in vitro cellular uptake and improved stability.* Acta Biomater, 2015. **28**: p. 149-159.

16. Zhang, L., et al., *Folate-modified lipid–polymer hybrid nanoparticles for targeted paclitaxel delivery.* International journal of nanomedicine, 2015. **10**: p. 2101.

17. Domingues, N.J.A., *Carrier Systems for Vitamin D.* 2013.

18. Brożyna, A.A., et al., *Expression of vitamin D receptor (VDR) decreases during progression of pigmented skin lesions.* Hum Pathol, 2011. **42**(5): p. 618-631.

19. Brożyna, A.A., et al., *Expression of Vitamin D-Activating Enzyme 1α-Hydroxylase (CYP27B1) Decreases during Melanoma Progression.* Hum Pathol, 2013. **44**(3): p. 374-387.

20. Scopel, R., et al., *Lipid-polymer hybrid nanoparticles as a targeted drug delivery system for melanoma treatment.* INTERNATIONAL JOURNAL OF POLYMERIC MATERIALS AND POLYMERIC BIOMATERIALS, 2022. **71**(2): p. 127-138.

21. Verderio, P., et al., *Intracellular Drug Release from Curcumin-Loaded PLGA Nanoparticle Induces G2/M Block in Breast Cancer Cells.* BioMcromolecules, 2013. **14**: p. 672-682.

22. Bivash Mandal, M., et al., *Core–shell-type lipid–polymer hybrid nanoparticles as a drug delivery platform.* nanomedicine, 2013. **9**: p. 474-491.

23. Yang, Z., et al., *Targeted delivery of 10-hydroxycamptothecin to human breast cancers by cyclic RGD-modified lipid–polymer hybrid nanoparticles.* Biomedical Materials, 2013. **8**.

24. Danquah, M., et al., *Combination Therapy of Antiandrogen and XIAP Inhibitor for Treating Advanced Prostate Cancer.* Pharm Res, 2012. **29**: p. 2079-2091.

.

Biomaterials Journal
http://www.biomatj.com
Online ISSN: 2812-5045

Type of the Paper (Editorial)

Recent Smart Dental Materials

Tamer M. Hamdy [1,*]

[1] Restorative and Dental Materials Department, Oral and Dental Research Institute, National Research Centre (NRC), Giza, Dokki, 12622, Egypt
* Corresponding author e-mail: dr_tamer_hamdy@yahoo.com

Citation: Tamer M. Hamdy. ***Recent Smart Dental Materials***. *Biomat. J., 2 (1),40 – 41 (2022).*

https://doi.org/10.5281/znodo.5829408

Received: 29 January 2023
Accepted: 30 January 2023
Published: 31 January 2023

Abstract: Smart materials have an integral competence to sense and react according to the variations in the environment. They can respond to the stimuli and changes in the surrounding environment by activating their functions accordingly and hence they are termed as" responsive materials". These materials have properties that can be altered in a measured way by stimuli such as stress, temperature, moisture, pH, electric, or magnetic fields. Several smart dental materials present recently in dental market such as smart resin composite, glass ionomer, pit and fissure sealants, endodontic instrument, orthodontic wires, silicone elastomer, bite registration material and thermochromic toothbrushes. These materials would potentially provide an innovative dental service with enhanced clinical outcome of the handling procedures.

Keywords: Smart, Biomimetic, bioresponsive, biosmart dentistry, materials.

Smart materials have an integral competence to sense and react according to the variations in the environment. They can respond to the stimuli and changes in the surrounding environment by activating their functions accordingly and hence they are termed as" responsive materials". These materials have properties that can be altered in a measured way by stimuli such as stress, temperature, moisture, pH, electric, or magnetic fields. Several smart dental materials present recently in dental market such as smart resin composite, glass ionomer, pit and fissure sealants, endodontic instrument, orthodontic wires, silicone elastomer, bite registration material and thermochromic toothbrushes.

These materials would potentially provide an innovative dental service with enhanced clinical outcome of the handling procedures.

Smart materials sense changes in the environment around them and responds in a predictable manner. In general, these features are:

Piezoelectric: when a mechanical stress is applied, an electric current is generated; Shape memory: can change the shape whenever required and can return back to original shape once force and pressure applied is removed; Thermo-chromic: these materials change color in response to changes in temperature; Photo-chromic: these materials change color in response to changes in light conditions; Magneto-rheological: these are fluid materials become solid when placed in a magnetic field; pH sensitive: when pH of the surroundings gets changed they will change their shape; Biofilm formation: presence of biofilm on the surface of material alters the interaction of the surface with the environment.

With developments in dental research, Novel dental materials have made their way into the dental market. Each newer restorative material introduced has its set of benefits and shortcomings. Restorative materials should be carefully chosen based on the clinical condition and requirements of the tooth to be restored. Clinician should have a thorough

understanding of the indications, contraindications, advantages and disadvantages of the dental material being used by them. This editorial provides a highlight to understand of the recent advancements and modifications in field of dental materials.

Biomaterials Journal
http://www.biomatj.com
Online ISSN: 2812-5045

Type of the Paper (Editorial)

Bioactivity of Dental Materials

Tamer M. Hamdy [1,*]

[1] Restorative and Dental Materials Department, Oral and Dental Research Institute, National Research Centre (NRC), Giza, Dokki, 12622, Egypt
* Corresponding author e-mail: dr_tamer_hamdy@yahoo.com

Citation: Tamer M. Hamdy.***Bioactivity of Dental Materials***. *Biomat. J., 2 (1),42 – 43 (2022).*

https://doi.org/10.5281/znodo.5829408

Received: 29 January 2023
Accepted: 30 January 2023
Published: 31 January 2023

Abstract: Bioactive dental materials not considered as a novel idea. Adhesion of dental materials into hard dental structure by an appetite-like deposition by help of fluoride releasing materials or by interaction of calcium phosphate-based materials considered as the first step for bioactivity. As there are materials have been widely used over many years that demonstrated numerous levels of bioactivity. These materials are used mostly for repair, reconstruction and regeneration of dental invectives. For example, glass ionomer has been described as bioactive material due to their capability to remineralization the demineralized tooth structure, furthermore to continuous dynamic release of fluoride ions which delay the secondary caries around the restoration margins.

Keywords: Bioactive, remineralization, bone formation, regeneration.

Bioactive dental materials not considered as a novel idea. Adhesion of dental materials into hard dental structure by an appetite-like deposition by help of fluoride releasing materials or by interaction of calcium phosphate-based materials considered as the first step for bioactivity. As there are materials have been widely used over many years that demonstrated numerous levels of bioactivity. These materials are used mostly for repair, reconstruction and regeneration of dental invectives.

For example, glass ionomer has been described as bioactive material due to their capability to remineralization the demineralized tooth structure, furthermore to continuous dynamic release of fluoride ions which delay the secondary caries around the restoration margins.

Moreover, calcium hydroxide, which have used for decades can be dissociated into calcium and hydroxyl ions, which in turn cause cascade of events that inspire deposition of reparative dentin and tooth remineralization. Therefore, these activities make glass ionomer and calcium hydroxide one of the firstly known bioactive dental materials. Bioactive dental materials could be defined as materials that form a layer of an appetite-like deposits at the tissue materials boundary upon exposure to inorganic phosphates solution.

Mechanisms of bioactivity includes a different step may occurs alone or together. A bioactive restorative material comprises at least one or more of the following behaviors; 1. Remineralization of the hard-dental tissues through fluoride and or other minerals release; 2. Apatite-like formation along the material tissue interface upon immersion in liquid; 3. Tissues repair and regeneration by encouraging the normal healing mechanism.

The level of evolution will comprise extended applications across all dental material categories, including permanent fillings, adhesives, dental and bone cements, bone grafts, substitute and scaffold, cavity liners and bases, endodontic sealers and pulp capping, preventive measures and patient home care. Bioactivity raises to a inimitable property of a material that provokes a cellular response, such as the formation of

hydroxyapatite. As compared to inert materials, bioactive materials are capable to produce growth factors and encourage natural mineralization. These responses has a large impact on the mechanically and esthetically results, thereby clinical durability of the bioactive material.